# Modelling of radionuclide retention by matrix diffusion in a layered rock model - response to the request by SSM for supplementary information on retention of radionuclides (SSM2011-2426-110), items 4 and 6.

Martin Löfgren – Niressa AB

James Crawford – Kemakta Konsult AB

2014-01-30

# Contents

# 1 Introduction

This report summarises the strategy and setup of, and results from, radionuclide transport modelling that is complementary to the modelling performed within the SR-Site safety assessment. The primary aim is to investigate whether the simplifications made in SR-Site calculations, concerning radionuclide retention by matrix diffusion in the rock surrounding flowpaths, are adequate. This report should be seen as a response to SSM's request for supplementary information on retention of radionuclides (SSM2011-2426-110), relating to items 4 and 6. If translating these items from SSM2011-2426-110, they read:

> 4. SSM considers that SKB should produce an analysis of the effect of mineral alterations and fracture-filling minerals in the rock on matrix diffusion and retardation of radionuclides. The analysis should highlight both the processes and characteristics that could mean improved or deteriorated retardation relative to the base case where the undisturbed rock is considered.[1]
>
> 6. SSM considers that SKB should analyse the importance of reasonably probable variability of the rock diffusivity and its impact on radionuclide transport.[2]

In SSM2011-2426-110, SSM provides further reasoning behind the requested items, which has been used as guidelines when planning this response. Based on this information, SKB has made the interpretation that the focus of the complementary modelling study should be on matrix diffusion, and not on sorption. Consequently, in the performed modelling, matrix diffusion properties are varied while sorption properties are held constant.

In the modelling study, we have conceptualised the flowpath adjacent rock at Forsmark to consist of up to three layers, perpendicular to the fracture surface, each having individual matrix diffusion properties. These layers are 1) fracture coatings; 2) alteration rim; and 3) undisturbed rock. It is assumed that the same layers do not persist along the entire flowpath, but that the flowpath encounters sections of different layer properties. This approach should be compared with the pessimistic modelling approach of SR-Site, which in practise assumes that the flowpaths are directly bounded by undisturbed rock (SKB 2010a).

In this response, we provide a best estimate matrix diffusion parameterisation of the three layer rock model, and its variation along typical flowpaths. This has been done in spite of the fact that there exist little, or no, site specific information on certain matrix diffusion parameters for the fracture coatings and rock directly adjacent to flowpaths. By using the assumed three layer rock model, we have performed complementary radionuclide transport modelling that incorporates data and assumptions from the SR-Site scenario giving rise to the highest radiological risk[3]. Both the SR-Site approach of

---

[1] *"4. SSM anser att SKB bör ta fram en analys av hur mineral-omvandlingar och sprickfyllnadsmineral i berget påverkar matrisdiffusion och retardation av radionuklider. Analysen bör belysa både processer och egenskaper som kan innebära förbättrad respektive försämrad retardation i förhållande till grundfallet där det opåverkade berget beaktas."*

[2] *"6. SSM anser att SKB bör analysera betydelsen av rimlig sannolik variabilitet av bergets diffusivitet och dess inverkan på radionuklidtransport."*

[3] Residual scenarios and future human action scenarios have not been considered.

bounding flowpaths by undisturbed rock and the approach of using the three layer rock model have been modelled, and the results are compared. To deal with the substantial uncertainty in matrix diffusion properties of the fracture coating and alteration rim layers, as well as to respond to some of SSM's concerns, modelling of a five variant cases have been performed.

When originally planning this response, we underestimated the effort and time needed to properly conceptualise the layered rock model, to parameterise it, to adapt the computational code, and to perform the numerical modelling. As a result, fewer radionuclides than originally intended have been internalised in the modelling, and a simplified version of the source term has been used. In addition, fewer variant cases than initially intended have been modelled. Importantly, even under these limitations, the modelling results in combination with the conceptual understanding of matrix diffusion strongly indicate that the gain of using a layered rock retention model, compared to using the SR-Site approach, is small. This is not an unexpected conclusion, and is in line with previous work on the matter (Cvetkovic 2010, Selroos and Painter 2012). Both approaches produce similar retention results, where the SR-Site approach produces slightly higher doses. Consequently, in respect to radionuclide retention by matrix diffusion, the SR-Site approach is judged to be pessimistic and, hence, adequate.

# 2 Conceptualisation of rock adjacent to flowpaths

In the few safety assessments that have internalised a layered or stratified structure in the rock, e.g. TILA-99 (Vieno and Nordman 1999, Section 11.5) and TURVA-2012 (Posiva 2013, Section 7.8), the rock directly adjacent to the flowpaths has been assigned a larger effective diffusivity and porosity than the undisturbed rock. In other safety assessments, matrix diffusion has only been allowed for in the alteration rim around fractures, while diffusion into the undisturbed rock has been conservatively neglected. This indicates either the assumption of a lower relative diffusion resistance[4] in the fracture adjacent rock, compared to that in the undisturbed rock matrix, or that deeper penetration was not "needed" in the modelling to achieve the assessment goals. A summary of how matrix diffusion is handled in eight safety assessments between 1983 and 1999 is given in SKB (2004, Section 4.3).

There is a large body of experimental evidence supporting the notion of layered rock at water bearing fractures, where the outmost layers facing the fracture have decreased relative diffusion resistances. Significant evidence comes from $^{14}$C-PMMA impregnations demonstrating that some of the most common fracture minerals, e.g. chlorite and clay minerals, have high and accessible porosities (e.g. Penttinen et al. 2006a, b, Siitari-Kauppi et al. 2010, Widestrand et al. 2007, 2010). This would indicate that they have a low relative resistance towards matrix diffusion, although this has not been generally verified (or disproved) by laboratory diffusion experiments. Diffusion into fracture coatings plays the leading role for in situ tracer tests in flowing water performed in fractured crystalline rock. As such tests are short termed, they target fracture fillings and little penetration into the underlying rock matrix is achieved. In Zhou et al. (2007) a literature survey covering 40 field tracer tests at 15 geological sites is presented, with regard to the field-scale effective matrix diffusion coefficient (i.e. the effective diffusivity). The lower limit of the estimated effective diffusivity range, from all these field-scale tracer tests, is $3 \cdot 10^{-12}$ m$^2$/s. This should be compared to the effective diffusivity of the underlying rock matrix, which may be orders of magnitude lower. For example, in SR-Site the best estimate effective diffusivity of the undisturbed in situ rock is assumed to be on the order of $10^{-14}$ m$^2$/s.

Concerning the alteration rim, that is the rock volume where alteration processes have occurred as response to flowing water in the adjacent open fracture, there is ample evidence from $^{14}$C-PMMA impregnations, and in some instances from laboratory diffusion experiments (e.g. Vilks et al. 2005, Widestrand et al. 2007, Selnert et al. 2008), that its relative resistance towards matrix diffusion should be lower than in the undisturbed rock. There is also a process based understanding of the generally increased porosity, as certain minerals are dissolved in alteration processes, which results in a residual void (e.g. SKB 2010b, Section 5.5, Siitari-Kauppi et al. 2010). However, it is a simplification to conceptualise the alteration rim as a layer of constant properties. It is rather a zone of increased porosity that gradually reaches the matrix diffusion properties of the underlying undisturbed rock matrix, as the distance from the fracture increases. The thickness of this zone is often reported to be on the order of a centimetre. It should

[4] With relative diffusion resistance, we mean the absolute diffusion resistance in relation to the layer thickness.

be noted that the thickness of the alteration rim in respect to other alteration observables, such as red staining of minerals by hematite precipitates, may be of limited value for determining the thickness of the alteration rim in respect to matrix diffusion properties.

When setting up a retention model, the layered rock structure can be assumed to have persistent retention properties along the entire flowpath. Alternatively, as we have done, the flowpath can be divided into different sections featuring layered structures of different properties. A conceptual image of this is shown in Figure 1, where a flowpath intersects two sections of layered rock. In our conceptualisation, the upper and lower rock volumes are mirror images of each other. The flowpath is in direct contact with a layer of fracture coatings, unique for each section. These in turn coat two types of alteration rims, which are in turn surrounded by two types of undisturbed rock. Each layer may be assigned individual thickness and retention properties, but the properties within a layer are assumed to be constant.

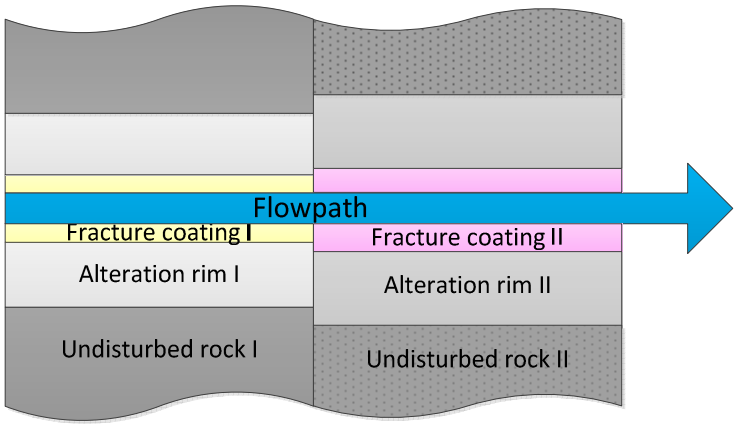


*Figure 1. Conceptual image of two rock volumes that a flowpath encounters; each having different layer diffusion properties and layer thickness. Layers such as these constitute the building blocks of our layered rock model.*

Figure 1 has similarities with, and can be seen as a simplification of, the well-known generalised conceptual model of the flowpath adjacent rock system established within the TRUE Block Scale project at the Äspö Hard Rock Laboratory, which is shown in Figure 2.

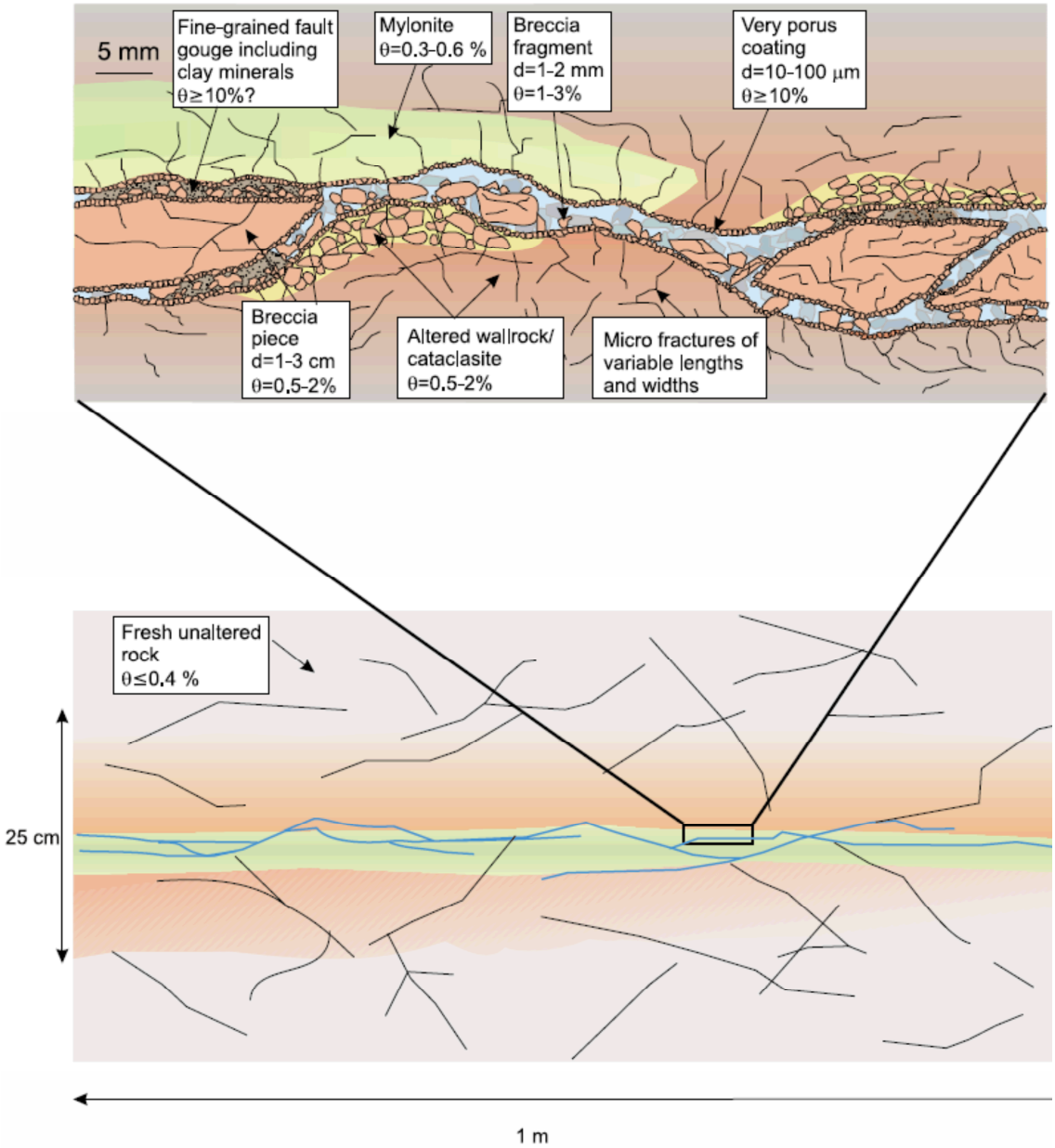


*Figure 2. Generalised conceptual model from the TRUE Block Scale project of a typical conductive structure involved in the tracer experiments. Details in the rock types etc. may not be representative for the Forsmark site. Reproduced from Winberg et al. (2003, Figure EX-2).*

# 3 Computational tool used in radionuclide transport modelling

In SR-Site, the bulk of the far-field radionuclide transport modelling was performed by the computational code FARF31 (SKB 2010a). For some special cases, the MARFA code v3.2.2 (Painter and Mancillas 2009) was used as a complement to FARF31, to investigate special features such as for segmented transport pathways featuring different rock types or hydrodynamic properties in each segment. As stated in SKB (2010a, Section 3.6.3), concerning MARFA:

> *"Limited and unlimited matrix diffusion, equilibrium sorption, longitudinal dispersion, decay, and in-growth are represented. MARFA supports full spatial variability for all pathway properties, decay chains of any length, and full temporal variability in radionuclide source strength."*

In the context of this present report, this means that one can assign different porosities and effective diffusivities to different sections of rock along a flowpath. As MARFA is a more versatile tool than FARF31, it has been chosen for the modelling leading up to this present report. The MARFA version used for this report, v3.2.3 (Painter and Mancillas 2013), is a new version relative to that used in SR-Site. It allows for the simulation of segmented flowpaths where the individual rock units can have up to three distinct microstructural layers featuring differing sorptive and diffusive properties (i.e. material properties varying perpendicular to the fracture plane). Each layer may be assigned individual porosity, $K_d$-values, effective diffusivities and thickness, although the parameters are constant within a layer.

It is recognised that the MARFA version used for this response is new, and has not been verified by SKB to the same extent as FARF31 and MARFA v3.2.2 have been. This requires extra care in examining potential modelling artefacts. To some extent this has been handled in the work leading up to this response, although the work does not fulfil the requirements of a formal verification. It should be noted, though, that this new version of MARFA was used in the recent Finnish safety case for a KBS-3 repository, TURVA-2012, which is a quality assured project.

# 4 The analysed scenario

## 4.1 SR-Site scenario used as starting point

A conclusion of the SR-Site safety assessment was that only a limited number of canisters are likely to fail during the analysed one million year time frame. If so, they are likely to fail due to copper corrosion as result of advective conditions in the deposition hole (e.g. SKB 2011, Figure 12-18). Such advective conditions will only occur in canister positions encountered by water conducting fractures of relatively high flow and low flow-related transport resistance. When setting up the MARFA model for this present modelling exercise, focus has been on the flowpaths associated with canister failure of the "central corrosion variant" of the "canister failure due to corrosion" scenario (SKB 2011, Section 13.5). Out of the scenarios with likelihood to occur, this particular scenario represents the highest radiological risk in SR-Site (SKB 2010a).

## 4.2 Choice of modelled flowpaths

In the "central corrosion variant" of the "canister failure due to corrosion" scenario in SR-Site, each canister was given a time of failure, based on careful considerations within other parts of the safety assessment. When choosing flowpaths for this present modelling exercise, we chose only from the pool associated with canister failure within the assessment time frame. Flow related data for the 56 canister positions included in this pool is shown in SKB (2010a, Table 4-3). Out of these, the following flowpaths have been selected:

1. The flowpath associated with the first canister failure.
2. The flowpath having the lowest F-factor.
3. The flowpath having the median F-factor.

For flowpaths in the upper F-factor range, the retention is so great that they become insignificant for the radiological risk, more or less regardless of modifications made in terms of retention parameters. For the selected flowpaths, the data of SKB (2010a, Table 4-3) are reproduced in Table 1.

**Table 1. Data for the deposition holes where canisters fail due to corrosion for the ten realisations of the semi-correlated DFN model. Data reproduced from SKB (2010a, Table 4-3).**

| Flowpath number | Time of failure (yr) | Rock transport resistance, F-factor (yr/m) | Advective travel time, $t_w$ (yr) | Advective flow through deposition hole, q ($m^3$/yr) |
|---|---|---|---|---|
| 1 | 114,485 | 53,660 | 6 | 0.733 |
| 2 | 803,247 | 11,330 | 20 | 0.035 |
| 3 | 201,037 | 89,910 | 17 | 0.144 |

As can be seen in Table 1, there is quite a difference in time of failure for the different flowpaths. Judging from SKB (2010a, Table 4-3) for the relatively early releases, the time of failure is better correlated to the advective flow through the deposition hole than to the F-factor. If internalising different times of failure in the modelling exercise, it would require individual source terms. This would complicate comparisons of

radionuclide releases from different flowpaths, and the impact of flow related and non-flow related transport properties of the host rock. This problem has been solved by assuming, for this particular modelling exercise, that the canisters of all three flowpaths fail at 114,485 years. By doing this, the source term associated with the canister that fails first, according to the SR-Site scenario, has been used for all canisters.

It should be noted that the transport problem is fully specified by the F-factor and advective travel time and that the flowpath length is only needed to specify flowpath dispersivity (since MARFA requires input in the form of dispersion length if hydrodynamic dispersion is modelled). For the modelling presented here, hydrodynamic dispersion is neglected. For comparison, the flowpath length of flowpath 1, which was of special interest for deterministic calculations of the central corrosion case[5] in SKB (2010a, Section 4.4) is 650 m. Modelling results from the flowpaths of Table 1 are judged to encompass the entire range of impacts of the variable microporous structure on radionuclide fluxes, of relevance for the SR-Site radionuclide transport and dose modelling.

## 4.3 Choice of radionuclides, source term, and other assumptions

For the purpose of demonstration calculations, a number of important dose determining nuclides from SR-Site were selected (I-129, Se-79, Ni-59, and Ra-226). These nuclides represent a variety of sorbing characteristics ranging from non-sorbing to moderately sorbing. The source term is based on part of the source term of the central corrosion case of SR-Site (cf. Figure 4-2, SKB 2010a). In the central corrosion case, the dose contributions from the corrosion release fraction and the long-term constant release fraction due to fuel dissolution were modelled separately from the contribution from the instant release fraction. In this present exercise, the dose contribution from the instant release fraction has not been modelled. The derivation of the source term, exiting the near field and entering the far field, is discussed in SKB (2010a). The abbreviated version of the source term, with the reduced set of nuclides, is shown in Figure 3 (time relative to repository closure) and Figure 4 (time relative to canister failure).

[5] In the remaining of this report the "central corrosion case" is used synonymously with the "central corrosion variant of the canister failure due to corrosion scenario".

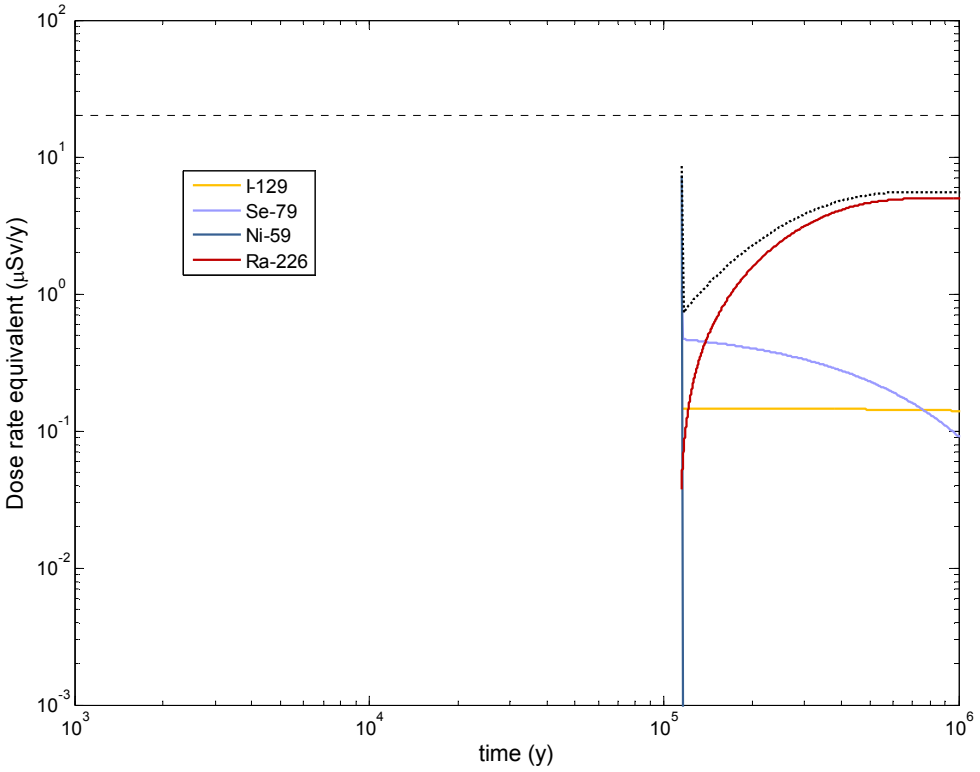


*Figure 3. Near-field dose equivalent release for deterministic calculations of the central corrosion case. The curve for Ni-59 is dominated by a fast corrosion release "spike", of which details are more visible in Figure 4.*

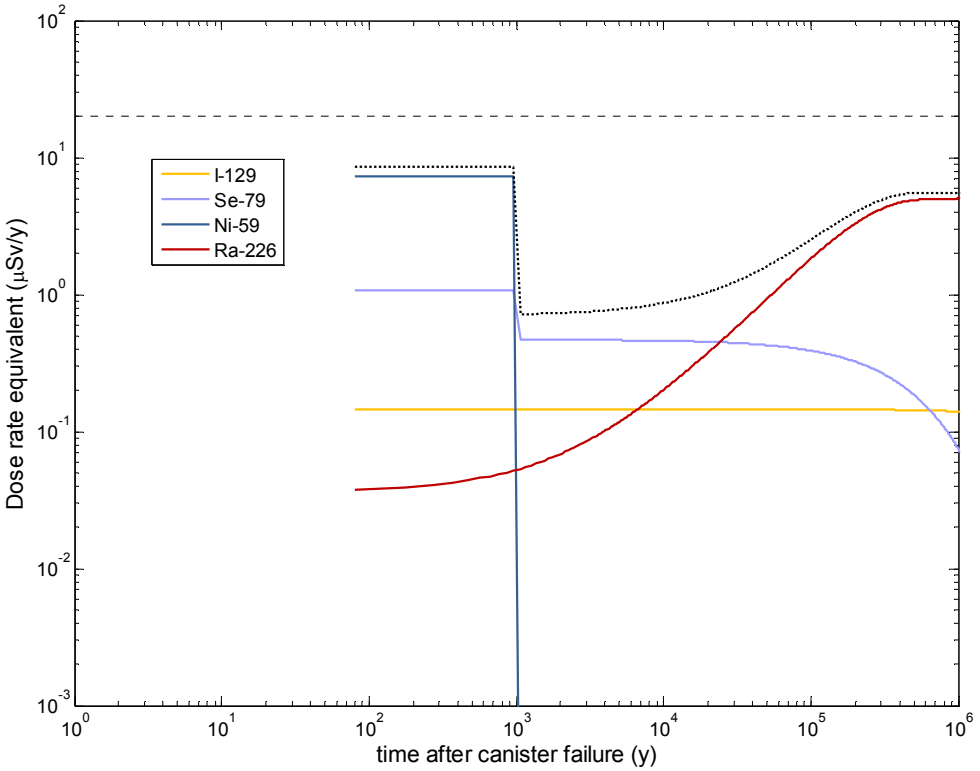


*Figure 4. Near-field dose equivalent release for deterministic calculations of the central corrosion case. The data are plotted in terms of time elapsed since canister failure and shows the source term for the Ni-59 nuclide more clearly.*

The identical source term has been assumed for each of the studied flowpaths, under the simplification that each canister fails at 114,485 years and has the same radionuclide inventory as the first failing canister in the central corrosion case. This simplification was judged to be necessary as it enables more transparent comparisons of radionuclide releases from different flowpaths. Furthermore, the simplification does not detract from the relative results where breakthrough curves for the layered rock model are compared with the reference case of undisturbed rock matrix from SR-Site.

In this modelling exercise, decay has been internalised but decay products and their migration have not been accounted for. When transforming radionuclide fluxes to effective dose rates, the basic landscape dose conversion factors of SKB (2010a, Table 3-7) have been used without further justification.

# 5 Parameterisation of the layered rock model – central case study

## 5.1 Dividing the flowpaths into fracture classes

In setting up the layered rock model for the central case study, the host rock has been divided into two main volumes. The first corresponds to the rock volume immediately surrounding the canister deposition holes and tunnels. This rock volume can be described by what is termed the immediate far field in Crawford (2008) and generally corresponds to the hydraulic rock domain. In this rock volume, the flowpaths are assumed to predominately occur in the discrete fracture network. As a rule of thumb, which we have adopted in the modelling, the F-factor in the immediate far field constitutes about 90% of the F-factor along the entire flowpath. As the flowpaths leave the immediate far field, they enter what we in this report call the distant far field. In this rock volume, flowpaths may to a larger degree be located in deformation zones, to which the deposition holes and tunnels have a respect distance. By assumption, the distant far field constitutes the last 10% of the flowpaths' entire F-factors.

To acknowledge that the properties of the layered rock are not persistent along the entire flowpath, we use four different fracture classes to set up our layered rock model. Three fracture classes, denoted fracture class 1:1, 1:2, and 1:3, are assigned to the immediate far field, while the forth (fracture class 2:1) is assigned to the distant far field. An illustration of this is provided in Figure 5 in Section 5.2. The first fracture class (1:1) features a fracture coating of low relative diffusion resistance and a moderate alteration rim. In this modelling exercise, we assume that the coating consist of a mixture of the commonly occurring fracture minerals chlorite and clay minerals, based on Byegård et al. (2008, Section 2.2.1) and Löfgren and Sidborn (2010). This fracture class is in line with how discrete fractures are usually perceived in sparsely fractured crystalline rock at depth, outside major deformation zones. The second fracture class (1:2) features no fracture coating and a week alteration rim. This fracture class has the foundation in the fact that open fractures with "fresh" rock surfaces have frequently been found when mapping the drill cores from the Forsmark site (e.g. Stephens et al. 2007, Eklund and Mattsson 2009).

The third fracture class (1:3) features a fracture coating made up of calcite. For this fracture mineral, or for the group of carbonate fracture minerals, there are contradicting observations. On the one hand there are observations from $^{14}$C-PMMA impregnations that calcite coatings are highly porous (e.g. Widestrand et al. 2010, Appendix 3). Such observations are in line with the parameterisation of the fracture coating layer of the calcite-coated transport class in the TURVA-2012 safety case (Posiva 2013, Table 7-14), which was assigned high porosity and effective diffusivity. On the other hand, there are observations from $^{14}$C-PMMA impregnations of fracture minerals that have a non-connected, or very poorly connected, porosity (e.g. Siitari-Kauppi et al. 2010). Such observations have been associated with calcite and carbonates. For the Forsmark site, there is no observation that could support either of these possibilities. Consequently, this is an uncertainty that must be handled by different modelling variants. As it is an unknown, the more pessimistic interpretation of the fracture coating has been internalised in the central case study; meaning that the calcite coating is assigned a low porosity and effective diffusivity. To not be overly pessimistic, only a

limited part of the flowpaths in the immediate far-field encounters this fracture class in the central case study.

In this modelling exercise, flowpaths in the distant far field are postulated to predominantly be associated with major fracture zones, which are represented by fracture class 2:1. Here the fracture surface is coated by relatively thick and porous fracture coatings and there exist a strong alteration rim of significant thickness. Accordingly, this fracture class has similarities with the investigated fractures in the TRUE series of experiments at Äspö (e.g. Winberg et al. 2003). For all four fracture classes, undisturbed rock is found beyond the alteration rim, with matrix properties equal to those assumed in SR-Site (SKB 2010c, Section 6.8).

## 5.2 Assigning retention properties to different layers

An illustration of our layered rock model, constituting four fracture classes and eleven different layers, is shown in Figure 5. The first data shown is the surface portion, which in the immediate far field corresponds to the portion of the flowpath's fracture surface that is represented by the fracture class. As discussed in Section 4.2, the transport problem is fully specified by the F-factor and advective travel time. Therefore, in the modelling, the surface portion of fracture class 1:1, 1:2, and 1:3 is multiplied by 90% of the flowpath's total F-factor (cf. Table 1), to get the fracture class specific F-factor. In the distant far field, that only features fracture class 2:1, the fracture class specific F-factor equals 10% of the flowpath's total F-factor.

The portion of the fracture surface that is represented by the fracture class is, for the immediate far field, based on the distribution of the fracture minerals chlorite, calcite, and clay minerals (counted as a group), as well as on the distribution of fresh fracture surfaces. Data on the occurrence and abundance of these fracture minerals are taken from a special campaign of quantitatively mapping fracture minerals of open fractures of drill cores from the Forsmark site, described in Eklund and Mattsson (2009) and Löfgren and Sidborn (2010). To obtain data tailored for this present modelling exercise, raw data from the campaign were revisited, as described in Appendix 2. Based on this, the surface portion and fracture coating layer thickness were estimated. Appendix 2 also provides more information on the procedure of deriving the parameter values of the other layers in Figure 5, in addition to the short description provided below.

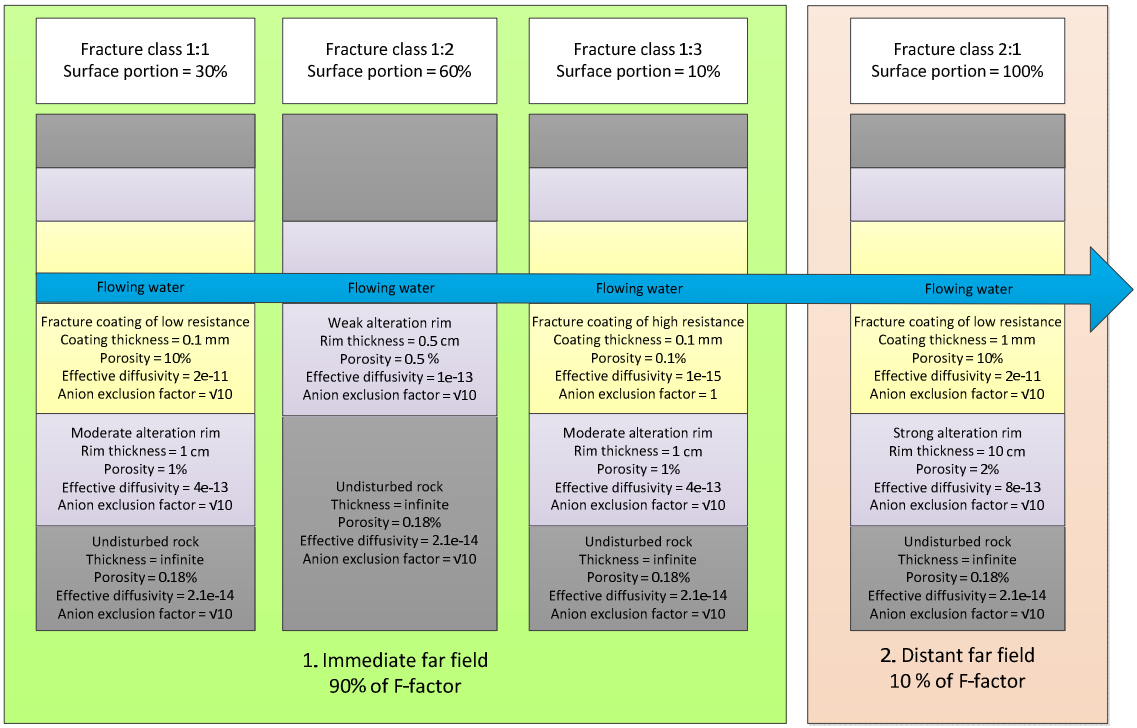


*Figure 5. Parameterisation of fracture classes and layers of the central case study. By the term "resistance" in the figure, the resistance towards matrix diffusive is meant. The upper fracture surface is a mirror image of the lower surface.*

Concerning the individual layers, the parameters used to describe their matrix diffusion properties are the layer thickness, the porosity, the effective diffusivity, and the anion exclusion factor. For the fracture coating layer and alteration rim, there exist almost no site specific data concerning their porosity and effective diffusivity. The site specific data that do exist, concerning rock directly adjacent to fractures, comes from six drill core pieces that were subjected to $^{14}$C-PMMA impregnation, providing information on its porosity distribution (Penttinen et al. 2006a). A few through-diffusion measurements have been performed on altered rock samples taken from within a meter of hydraulically conductive features (Selnert et al. 2008), but the rock samples may have been located many centimetres or decimetres away from the fracture, which may very well be too distant to impact the rock's matrix diffusion properties.

For the fracture coating layer and alteration rim, porosities have been estimated based on the above mentioned PMMA data from Forsmark, as well as on corresponding data from different sites of similar geological settings as Forsmark (Kelokaski et al. 2001, Penttinen et al. 2006a, b, Siitari-Kauppi et al. 2010, Widestrand et al. 2007, 2010, Kuva et al. 2012). For the alteration rim, account has also been taken of data from through-diffusion experiments on fracture adjacent Äspö rock (Vilks et al. 2005, Widestrand et al. 2007, 2010). When only the porosity has been available, the effective diffusivity has been estimated by relations such as the Archie's "law" (Archie 1942, Parkhomenko 1967) with the caveat that such relations have low precision in low-porous rock. For fracture class 2:1, data of the generalised conceptual model from the TRUE Block Scale project, shown in Figure 2, have been adopted.

For the undisturbed rock, the best estimate values of SR-Site are used for all fracture classes (cf. SKB 2010c, Tables 6-90 and 6-91). In SR-Site, an anion exclusion factor of half a $\log_{10}$-unit, or $\sqrt{10}$, was assigned to the undisturbed rock. This reduction factor was applied to the effective diffusivity, but not to the porosity. In this modelling

exercise we have adopted this reduction factor by applying it to the effective diffusivity of all layers of Figure 5, except for the fracture coating layer of fracture class 1:3. The reason is that the parameterisation of this layer is based on calcite layer properties. Calcite, which is a carbonate, has different charge properties compared to silicates and oxides. In case of calcite, the counter ions are hypothesised to be tightly bound to the surface in a very thin and non-diffuse double layer (e.g. Fenter et al. 2000). Based on this, the process of anion exclusion is assumed not to take place in this layer.

It could be argued that the data for the fracture coating and alteration rim layers are merely based on guesses, although the guesses are educated. Presently, without performing further experimental studies on site specific material, the only way to handle this uncertainty is by parameter variations in the modelling, or by applying pessimistic assumptions. The choice of data for the different layers, as shown in Figure 5, may be compared with the corresponding data for the Finnish safety case TURVA-2012 (Posiva 2013, Tables 7-13 to 7-16). In such a comparison, both similarities and deviations are found. The major deviation concerns the parameterisation of the calcite fracture coating layer in fracture class 1:3. Therefore, the TURVA-2012 parameterisation is used in a variant case for this layer, as further discussed in Chapter 7.

Concerning the $K_d$-values for the different layers, the simplistic approach of not assigning individual values for the different layers has been taken. Instead, the best estimate sorption coefficients of SR-Site, for undisturbed rock, have been used for all layers without further justification and without varying the $K_d$-values. These adopted values are shown in column two of SKB (2010c, Table 6-89). If it was the intention of SSM, expressed in item 4 of SSM2011-2426-110, that SKB should also vary retention properties associated with sorption, the presented layered rock model would be well-suited for such a modelling exercise. In that case, the greatest challenge would be to assign adequate $K_d$-values to the set of radionuclides in the different layers.

# 6 Results from the central case study

Figure 6 shows the resulting effective dose rate in μSv/yr for the three studied flowpaths (cf. Table 1). The horizontal dashed line shows the dose corresponding to the risk limit. The solid curves show the effective dose rates when assuming the layered rock model with the parameter values shown in Figure 5. The broken curves show the corresponding effective dose rates if using the SR-Site assumption that the entire flowpaths are directly bounded by undisturbed rock (cf. Figure 7 in the following chapter). The left panels of the figure show individual nuclide contributions to dose, while the right panels show the total summed dose for the modelled nuclides, for the particular flowpath. All plots in Figure 6 are magnified in Appendix 1.

If taking a general look at Figure 6, comparing different flowpaths, one can see that the F-factor impacts different nuclides differently. The F-factor varies by a factor of about eight between flowpaths 2 and 3 (cf. Table 1). For Ni-59, which is sorbing and is only released as a pulse during the first 1,000 years following canister breach, the F-factor has a great impact. Between flowpaths 2 and 3, the peak release rates of Ni-59 differ by little more than one order of magnitude. In fact, for flowpath 2, Ni-59 becomes the dominant dose contributor, even in comparison to Ra-226[6]. For I-129, which is non-sorbing and has a constant release rate after canister breach, the F-factor does not have a significant impact on the results. For R-226 that is sorbing and has an increasing release rate after canister breach, the impact of the F-factor on the peak release rate is a factor between three and five between flowpaths 2 and 3, depending on the studied case.

When comparing the results of the central case study and the SR-Site case for the same flowpath, the general difference in the effective dose rate curves is a delay in release to the surface system, as well as a reduction of the peak release rate for the central case study. The difference in conceptualisation of the two cases is associated with the very fracture adjacent rock, that is the fracture coating and alteration rim. Consequently, the greatest difference between the cases is expected for the leading edge of the pulse. The larger the portion of the pulse that has passed a certain position of the flowpath is, the thicker becomes the zone of the surrounding rock for which the rock storage capacity is occupied. As the storage capacity of the fracture coating and alteration rim becomes occupied, the retention starts to resemble the SR-Site case where the flowpaths are directly bounded by undisturbed rock. Consequently, the introduction of the layered rock model should have a greater reducing impact on the peak release rate for radionuclides of the corrosion release fraction (and instant release fraction) than for radionuclides constantly released due to fuel dissolution.

[6] Here it should be noted that we have assumed an earlier canister breach for flowpath 2 than in SR-Site.

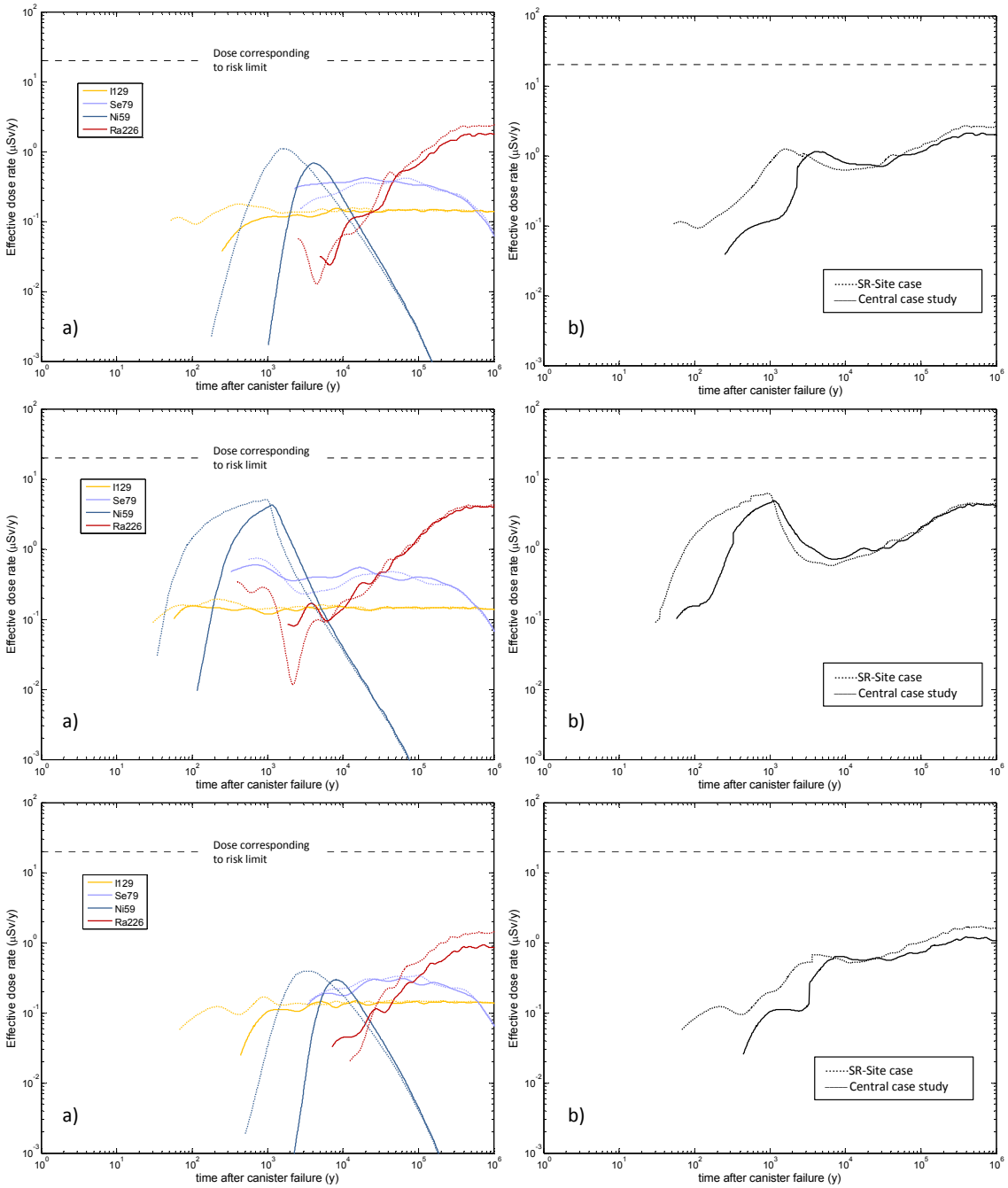


*Figure 6. Far-field dose rate results for flowpath 1 (upper), 2 (middle) and 3 (lower). Breakthrough curves for the SR-Site case of undisturbed rock matrix shown as broken lines; central case study shown as solid lines. Left panel shows individual nuclide contributions to dose; right panel shows total summed dose for modelled nuclides.*

For a more simplified case than modelled above, where the flowpath is bounded by only one fracture class, and where there is no decay, one would expect the difference for the leading part of the curves to be larger for non-sorbing species than for sorbing species. This is as the entire storage capacity is determined by the porosity for non-sorbing species, which is generally increased in the layered rock model (except for fracture class 1:3). For sorbing species, the porosity is only a part of the rock capacity and, hence, an increased porosity may be easily masked. However, as the solid curves of Figure 6 represent a relatively complicated case, their behavior becomes quite complicated to predict.

The complexity of the case also makes it difficult to deduce if the curves are affected by modelling artefacts, purely by visual inspection. To amend this, comparative modelling of some simplified cases has been performed to track down potential artefacts, although these additional simulations are not accounted for in this report. An important artefact that requires explanation is the apparent behavior of radionuclides having a limited near field release rate (cf. Figure 4). This primarily concerns I-129 and R-226 at early times, while Ni-59 is relatively unaffected. As can be seen for I-129 and R-226, the model erroneously predicts major fluctuations in the equivalent dose rate as the leading edge of the pulse reaches the surface system. This seems to be related to the stochastic nature of the particle tracking method used by MARFA and how far-field fluxes are calculated in the post processing algorithm. The rapid fluctuation might be due to the sensitivity of the calculation to the arrival times of the first few particles in the particle residence time distribution and how these are used to reconstruct the leading edge of the smoothed breakthrough curve.

# 7 Variant case studies

In this section, the setup of, and results from, variant case modelling are summarised. The general idea has been to adopt the three flowpath used in the central case study (cf. Table 1) together with the same assumptions on source term, decay, sorption, etc. (cf. Section 4.3). The flowpaths are then modelled as surrounded by layered rock, or non-layered rock, of different configurations and properties. It should be highlighted that the only input data that differ between the variant cases and the central case study concern the parameters shown in Figure 5. Apart from this, the models are identical.

## 7.1 The SR-Site case – entire flowpath surrounded by undisturbed rock

In SR-Site, a pessimistic modelling approach was adopted that in practise assumes that the flowpaths are directly bounded by undisturbed rock. Furthermore, for all practical purposes, unlimited pore connectivity was assumed. In this variant case these assumptions are adopted, as illustrated in Figure 7.

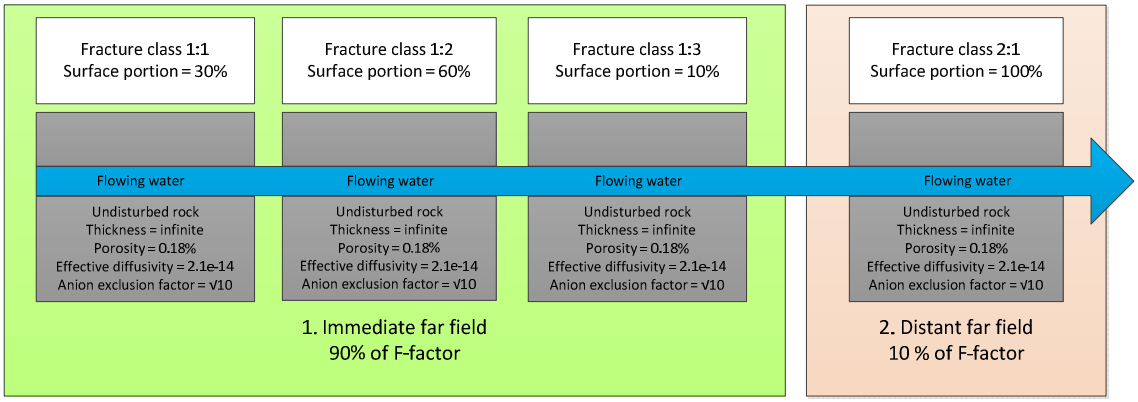


*Figure 7. Parameterisation of fracture classes and layers of the SR-Site case, where all layers feature undisturbed rock for both fracture surfaces.*

Results from this variant case have already been shown in Figure 6, by the broken curves. For flowpath 1, the equivalent dose rates correspond to those modelled in the central corrosion case in SR-Site (SKB 2010a, Figure 4-3), for the individual nuclides.

## 7.2 Layered rock with TURVA-2012 calcite coating case study

In fracture class 1:3, the fracture coating consists of calcite. As discussed in Section 5.1 (and Appendix 2), there are contradicting observations concerning the porosity of calcite as a fracture mineral. In some studies, the fracture mineral is observed to have a very low or non-connected porosity, while in others studies a high porosity is observed. In this case study, we keep the parameterisation of all layers as in Figure 5, with the exception for the fracture coating layer of fracture class 1:3. For this particular layer, the parameterisation assumed in TURVA-2012 for the calcite coating (Posiva 2013, Table

7-14) is used for the porosity and effective diffusivity. The modified layer, compared to the central case study, is highlighted by a red border in Figure 8.

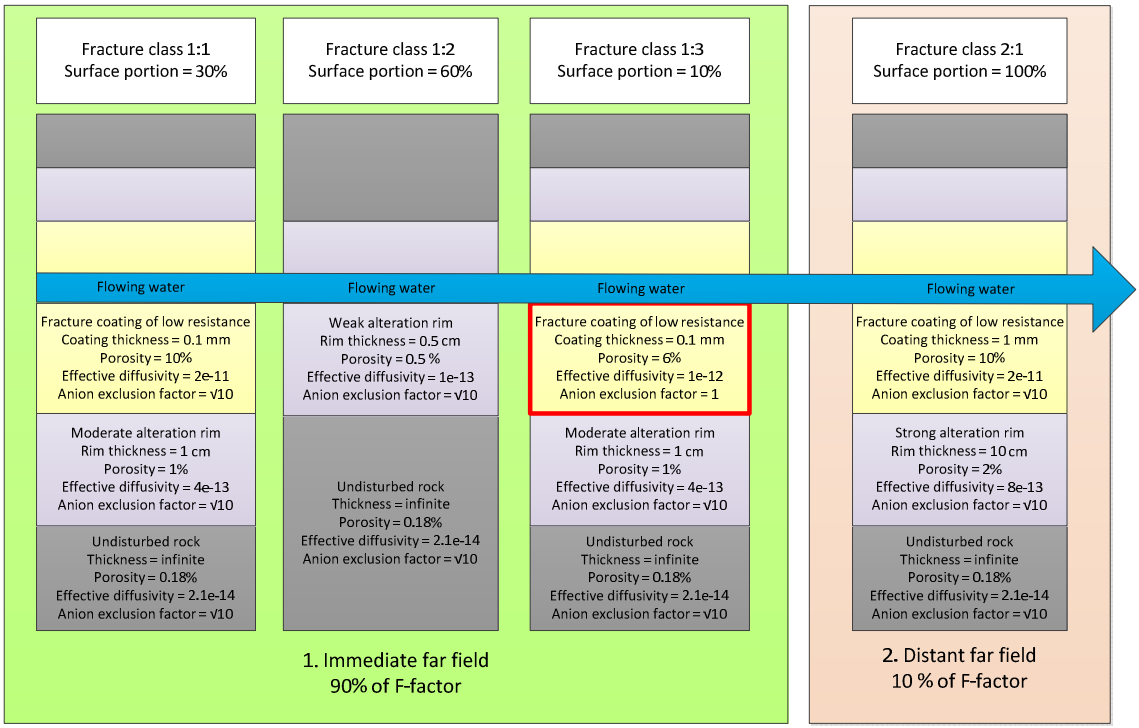


*Figure 8. Parameterisation of fracture classes and layers of the TURVA-2012 calcite case study. The upper fracture surface is a mirror image of the lower surface.*

This variant case can be used as an example of to what extent major changes in a single layer affect the results. It should be noted that for this layer, the effective diffusivity is increased by three orders of magnitude compared to the central case study. As only 10% of the F-factor is specific to fracture class 1:3, the impact on the dose may still be expected to be minor. Based on the prior discussion of how changes in matrix diffusion properties affect retention, the highest impact can be expected for the flowpath of the lowest F-factor (i.e. flowpath 2) and for non-sorbing or weakly sorbing species at the leading edge of the pulse. The modelling results are shown in Figure 9 for the three flowpaths, as compared to results from the central case study.

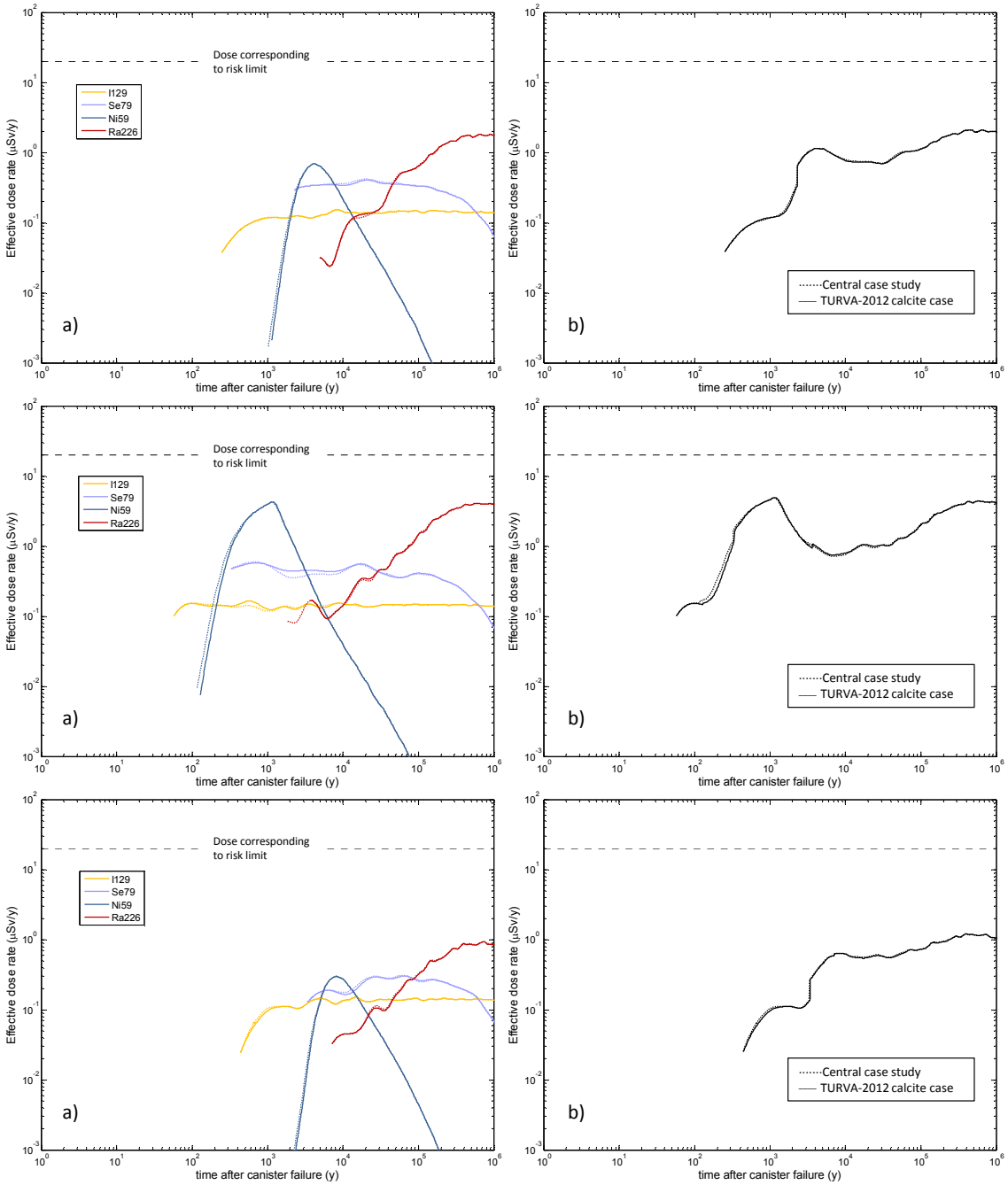


*Figure 9. Far-field dose rate results for flowpath 1 (upper), 2 (middle) and 3 (lower). Breakthrough curves for the central case study shown as broken lines; TURVA-2012 calcite case study shown as solid lines. Left panel shows individual nuclide contributions to dose; right panel shows total summed dose for modelled nuclides.*

As can be seen, the impact of the major changes in calcite diffusion properties is very minor. While one can detect a small difference for the leading edge of the pulse of flowpaths 2, other deviations can barely be seen.

## 7.3 Layered rock with limited pore connectivity case study

In SSM's reasoning behind item 4 in SSM2011-2426-110, the possibility of a limited maximum penetration depth for matrix diffusion is brought up. Such a limited maximum penetration depth would be associated with limited pore connectivity, or a microporous system at the percolation threshold (e.g. Haggerty 1999). To study the effect of a limited rock matrix, the parameterisation of the central case study is used, with the exception that the maximum penetration depth is limited to 10 cm. The few relevant long term in-situ experiments that exist have typically been carried out for long enough periods to achieve penetration on the decimetre scale (e.g. Birgersson and Neretnieks 1990, Möri et al. 2003, Vilks et al. 2004, Nilsson et al. 2010). Accordingly, it is a fair assumption that matrix diffusion can occur on, at least, this scale. As shown in Figure 10, this means a limitation of the thickness of the undisturbed rock layer for the fracture classes in the immediate far field. For the distant far field, the alteration rim thickness is slightly reduced and no penetration is allowed into the undisturbed rock.

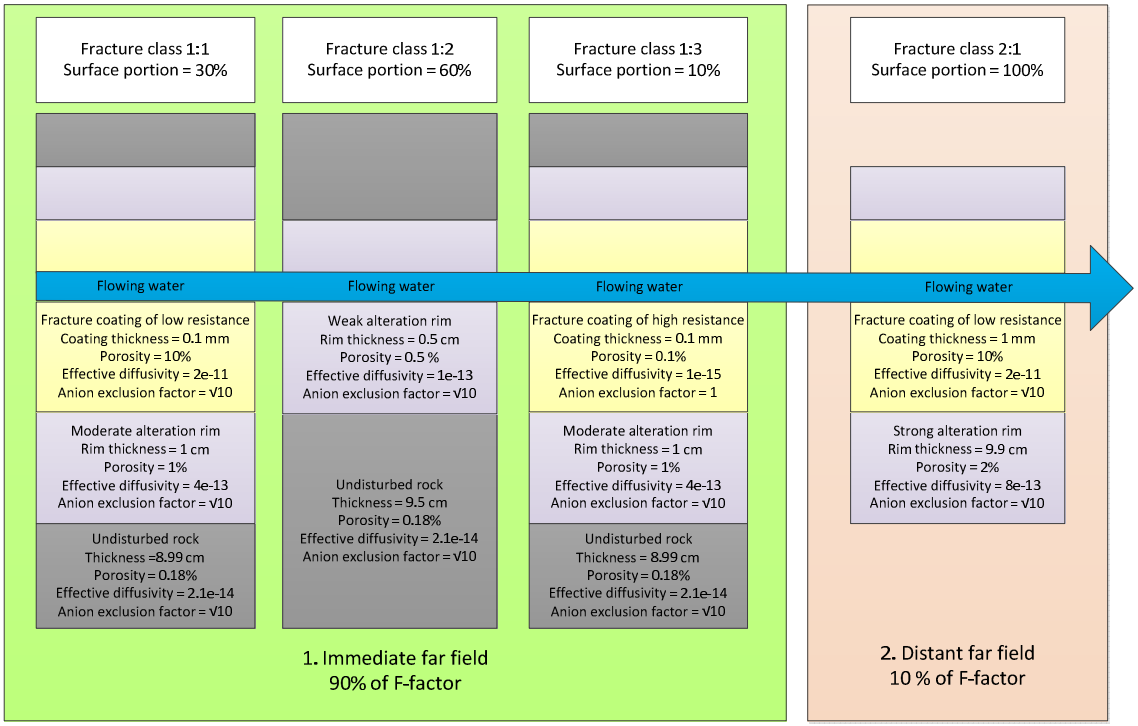


*Figure 10. Parameterisation of fracture classes and layers of the layered rock with limited pore connectivity case study. The upper fracture surface is a mirror image of the lower surface.*

The results from this case study are compared to results from the central case study in Figure 11.

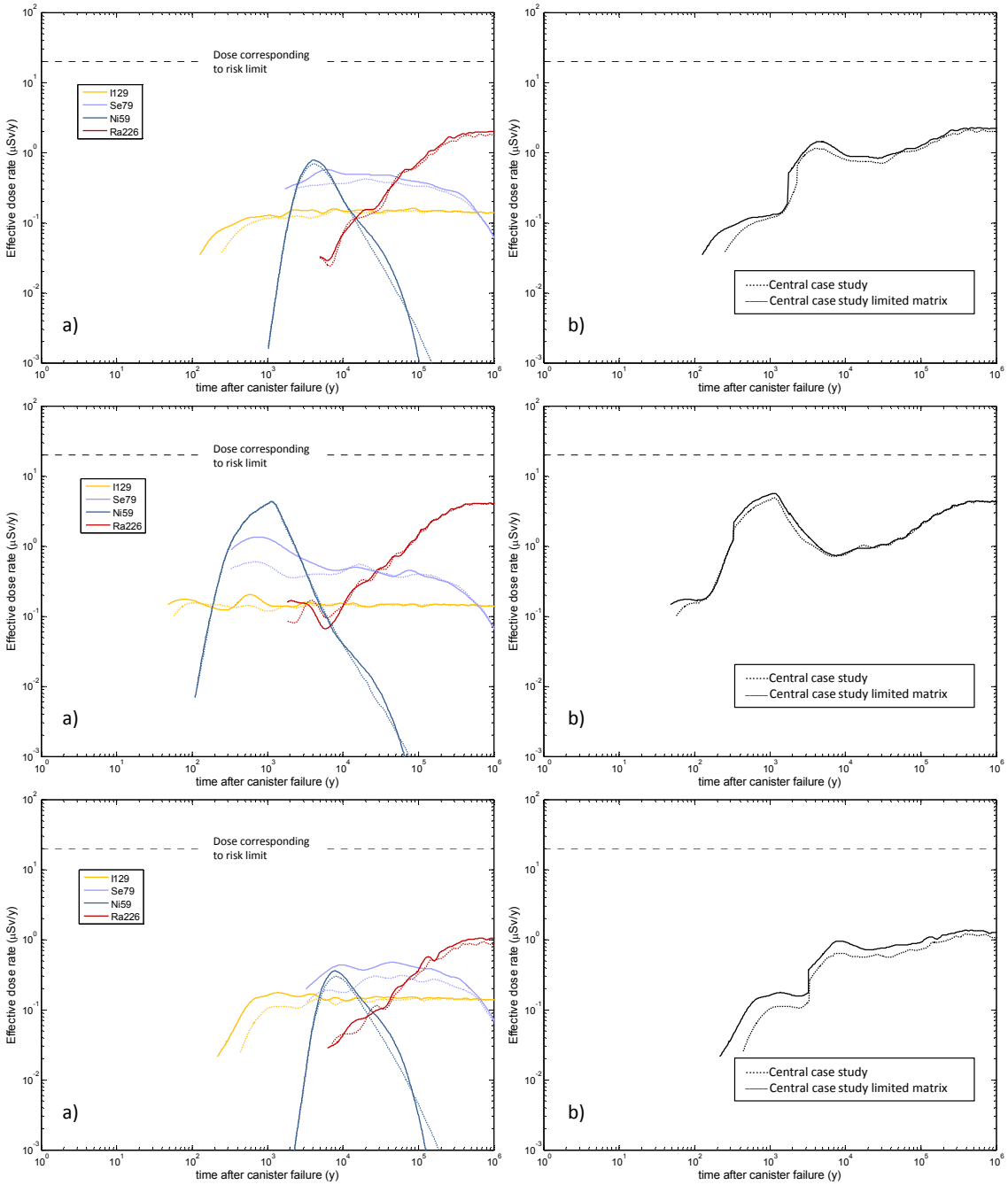


*Figure 11. Far-field dose rate results for flowpath 1 (upper), 2 (middle) and 3 (lower). Breakthrough curves for the central case study shown as broken lines; layered rock case study with limited pore connectivity shown as solid lines. Left panel shows individual nuclide contributions to dose; right panel shows total summed dose for modelled nuclides.*

When comparing the solid and broken curves of Figure 11, it should be kept in mind that all input data are identical for the two modelling cases, except for the limitation of the maximum penetration depth related to the solid curves. Accordingly, deviations between the two cases should signify that the radionuclide concentration at 10 cm depth into the rock matrix is sufficiently high to impact the driving force (i.e. the

concentration gradient) for matrix diffusion. When this happens, the retention decreases and the release curves are impacted. As the storage capacity of the rock is completely filled, no further retention is achieved. Accordingly, one can expect that a limitation of the rock matrix will affect the later part of the released pulse, and not the leading edge.

As can be seen from Figure 11, the expected outcome is not fully reproduced, especially at the leading edge of the curves (see previous discussion on modelling artefacts). Assuming that the peak release rates are approximately correctly predicted in Figure 11, one could say that limiting the maximum penetration depth to 10 cm has little impact on far-field dose rates in the safety assessment for the modelled F-factor range and assumed source term.

## 7.4 The SR-Site case but with limited pore connectivity

In this variant case, we use the same parameterisation as in the SR-Site case described in Section 7.1, but with the modification of limiting the maximum penetration depth to 10 cm. Accordingly, Figure 7 describes the case, if exchanging the layer thickness from infinite to 10 cm. The results from this case study are compared to results from the SR-Site case in Figure 12.

As for the former case study of limited connectivity (cf. Section 7.4), the expected results are not fully achieved for all release curves. For some release curves, such as for Se-79 in flowpath 3, the solid and broken curves are identical for the leading edge of the pulse, and gradually deviate as time progresses. At very late times, the curves for the nuclides associated with constant release source terms converge, as may be expected. However, for I-129 and flowpath 3, there is a deviation at the leading edge of the curve that does not appear to be caused by random fluctuation. It is recommended to revisit this issue at a later time. Under the assumption that the peak release rates are properly resolved in Figure 12, limiting the maximum penetration depth to 10 cm appears to have little impact on far-field dose rates in the safety assessment for the modelled F-factor range and assumed source term.

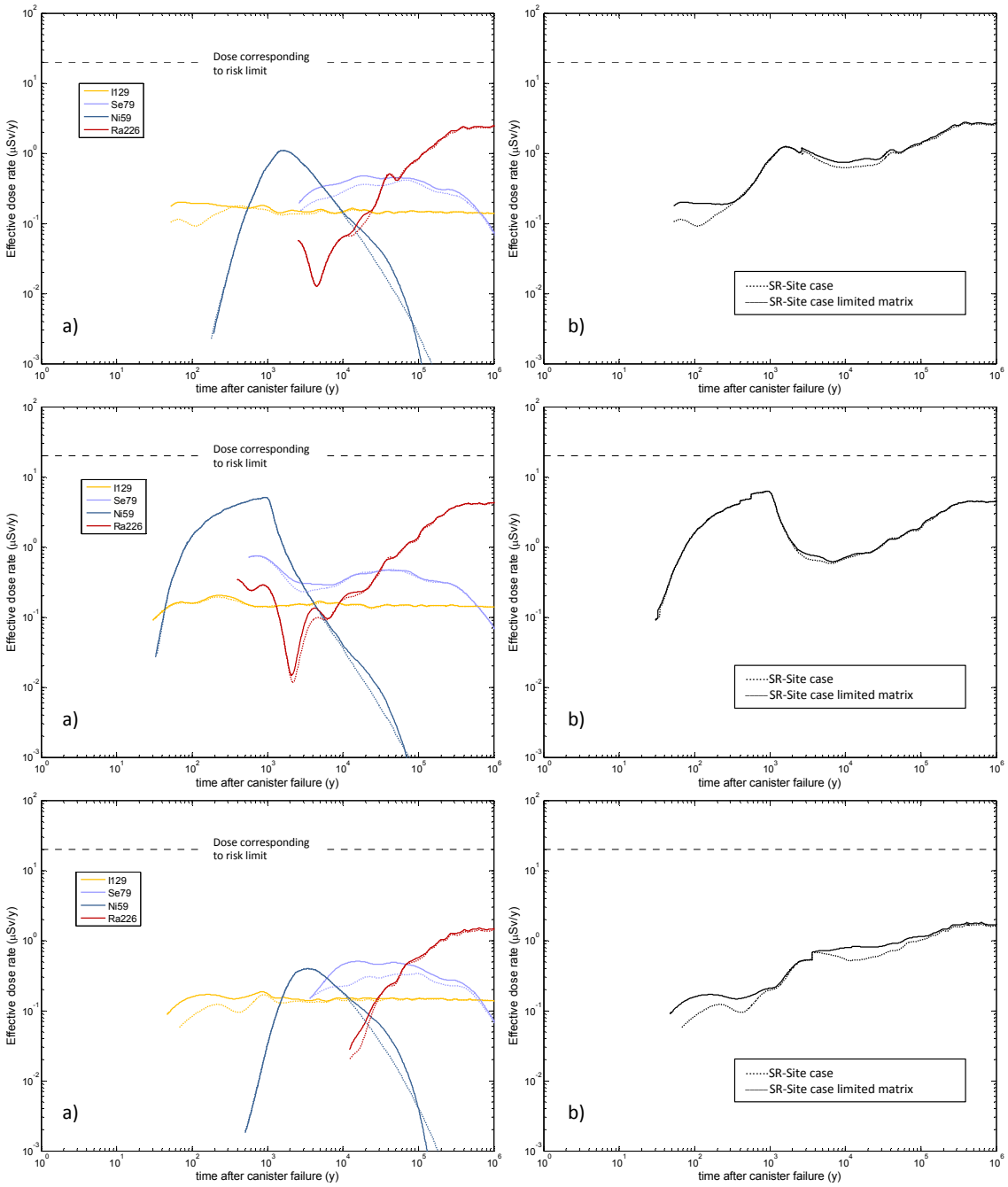


*Figure 12. Far-field dose rate results for flowpath 1 (upper), 2 (middle) and 3 (lower). Breakthrough curves for the SR-Site case shown as broken lines; SR-Site case with limited pore connectivity shown as solid lines. Left panel shows individual nuclide contributions to dose; right panel shows total summed dose for modelled nuclides.*

## 7.5 The SR-Site case but with reduced effective diffusivity

In item 6 of SSM's request, SKB is asked to analyse the importance of a reasonably probable variability of the effective diffusivity and its impact on radionuclide transport.

For the below discussion, the formation factor needs to be introduced. The relation between the formation factor $F_f$ (–) and the effective diffusivity $D_e$ ($m^2$/s) is:

$$D_e = F_f \cdot D_w \qquad \text{Equation 1}$$

where $D_w$ ($m^2$/s) is the diffusivity in unconstrained pore water. In SR-Site, it was assumed that the variability in the flowpath averaged formation factor, between flowpaths, is insignificant (SKB 2010c, Section 6.8). Hence, the variability in the effective diffusivity was largely contributed to the variability of the species' diffusivity in unconstrained pore water. Such variability in $D_w$ is due to the diffusing species' molecular weight, the temperature, and to a minor extent to the porewater composition, affecting the solution's viscosity. In SR-Site, element specific diffusivities in unconstrained pore water were not used for the geosphere. Instead a probability density function was introduced for the effective diffusivity, which should incorporate the variability in $D_w$, as well as possible minor bias in the flowpath averaged formation factor. The probability density function is given in Table 2.

**Table 2. Flowpath averaged in situ effective diffusivity suggested for use in SR-Site. Table reproduced from SKB (2010c, Table 6-91).**

| Type of solute | Best estimate $D_e$ ($m^2$/s) | $Log_{10}D_e$ ($m^2$/s) – $\mu$ | $Log_{10}D_e$ ($m^2$/s) – $\sigma$ | Probability density function |
|---|---|---|---|---|
| Cations and non-charged solutes | $2.1 \cdot 10^{-14}$ | –13.7 | 0.25 | Log-normal |
| Anions | $6.6 \cdot 10^{-15}$ | –14.2 | 0.25 | Log-normal |

Judging from item 6 of the request, SSM is concerned that the variability of the probability density function is too limited. This is handled in this variant case by pessimistically assuming that the effective diffusivity is one order of magnitude lower than in SR-Site. Based on the distribution in Table 2, this would mean an effective diffusivity four standard deviations below the best estimate value of SR-Site. In this variant case we use the same parameterisation as in the SR-Site case described in Section 7.1 and Figure 7, but with the change of effective diffusivity from $2.1 \cdot 10^{-14}$ $m^2$/s to $2.1 \cdot 10^{-15}$ $m^2$/s. The results from this case study are compared to results from the SR-Site case in Figure 13.

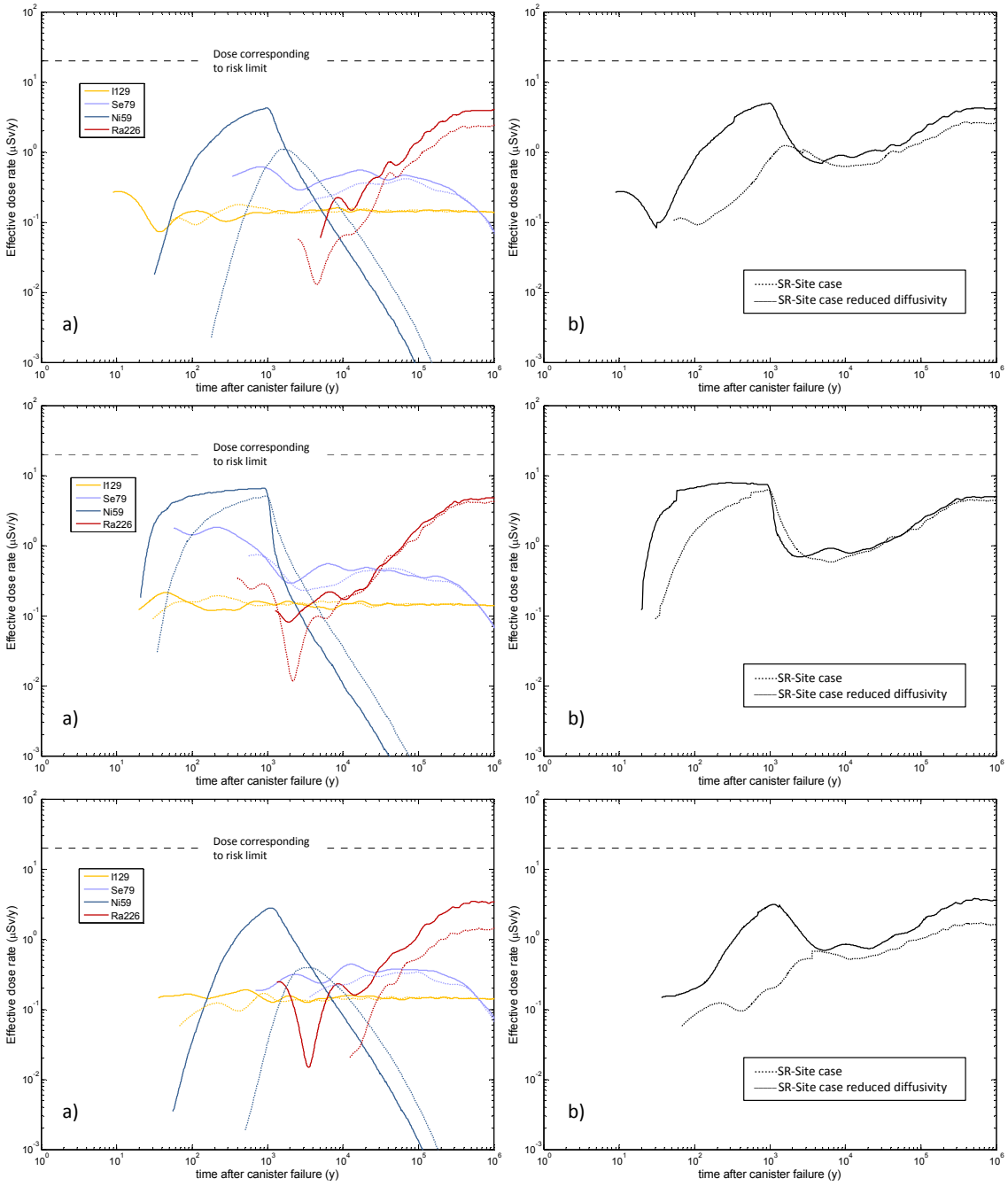


*Figure 13. Far-field dose rate results for flowpath 1 (upper), 2 (middle) and 3 (lower). Breakthrough curves for the SR-Site case shown as broken lines; SR-Site case with reduced effective diffusivity shown as solid lines. Left panel shows individual nuclide contributions to dose; right panel shows total summed dose for modelled nuclides.*

# 8 Conclusions

In this work a more complex representation of rock matrix diffusive properties has been used than that previously adopted in SR-Site. Flowpaths in the rock matrix are assumed to encounter a number of different rock volumes with differing matrix retention properties conceptualised as a discretely layered rock matrix (here taken to include fracture coatings). By introducing layers of different properties, a much larger range of matrix diffusion properties is accounted for than in SR-Site. Accordingly, we have increased the natural variability (which is sometimes discussed in terms of input data uncertainty) of the porosity and effective diffusivity as requested in SSM2011-2426-110.

Generally, the fracture surface is assumed to be bounded by fracture adjacent layers of higher porosity and effective diffusivity than the undisturbed rock. This is expected to give a more pronounced transport retardation compared to the SR-Site case, where the flowpaths were assumed to be bounded by undisturbed rock. The modelling results support this notion, as the modelled peak equivalent dose rates are generally lower in the central case study compared to the SR-Site case. In safety assessment, the peak release rate takes on special importance. The results show that by introducing the layered rock model, with realistic parameter values, the peak release rate is lowered by a factor of less than three, for the flowpaths considered. While this may be significant for the safety assessment, the reduction in dose is still minor. Here it should be noted that the instant release fraction was not modelled, and that its reduction in peak release rate is expected to be greater than this, if using a layered rock model.

The consideration of a range of different F-factors, representative of fast migration paths associated with failed canisters in the central corrosion case of SR-Site, revealed that the F-factor impacts different radionuclides differently, with respect to retention by matrix diffusion. This has partly to do with sorption properties of the nuclides considered and partly to do with the shape of the near field release source term. A small deviation in F-factor, say differing by a factor of about five, would seemingly impact the far field release rate more than our changes of the matrix diffusion properties, from the SR-Site case to the central case study.

In the central case study, unknowns concerning the diffusive properties of calcite coatings required us to incorporate a calcite coating layer of lower porosity and effective diffusivity than the undisturbed rock, in fracture class 1:3. However, as calcite covers such a small part of the fracture surface (10%), this had little impact on the results. This is shown in Figure 9 where the results are compared to an identical case, apart from the increased diffusive properties of the calcite coating. By changing the effective diffusivity by three orders of magnitude for a single layer, the equivalent dose rates of the far field release barely changed.

As the central case study produces lower far field release rates than the SR-Site case, a small number of variant cases were modelled, with the aim at applying pessimistic assumptions compared to either the SR-Site case or the central case study. This was mainly done by limiting the maximum penetration depth to 10 cm; or by reducing the effective diffusivity of the undisturbed rock by one order of magnitude. Limiting the maximum penetration depth had little impact on the release rates. As some parts of the

release curves may be affected by computational artefacts, more detailed conclusions cannot presently be made.

Reducing the effective diffusivity of the undisturbed rock by one order of magnitude did have a significant impact on peak release rates in different parts of the release curve (although by less than an order of magnitude), compared to the SR-Site case (cf. Figure 13). However, it should be kept in mind that there is little ground for assuming an effective diffusivity as low as $2.1 \cdot 10^{-15}$ $m^2/s$, even for in situ conditions. The effective diffusivity used in SR-Site for the in situ undisturbed rock is already low compared to what is used in other, equivalent, safety assessments (e.g. Posiva 2013, Section 7.8.2).

In summary, it is reasonable to say that the SR-Site approach of assuming flowpaths directly bounded by undisturbed rock is pessimistic relative to the adoption of a more realistic rock matrix microstructure in radionuclide transport calculations. This conclusion regards retention by matrix diffusion only, and not necessarily the combined retention due to matrix diffusion and sorption.

# References

**Archie G E, 1942.** The electrical resistivity log as an aid in determining some reservoir characteristics. Petroleum Transactions of AIME 146, 54–62.

**Birgersson L, Neretnieks I, 1990.** Diffusion in the matrix of granitic rock: field test in the Stripa mine. Water Resources Research 26, 2833–2842.

**Byegård J, Selnert E, Tullborg E-L, 2008.** Bedrock transport properties. Data evaluation and retardation model. Site descriptive modelling, SDM-Site Forsmark. SKB R-08-98, Svensk Kärnbränslehantering AB.

**Crawford J (ed), 2008.** Bedrock transport properties Forsmark. Site descriptive modelling, SDM-Site Forsmark. SKB R-08-48, Svensk Kärnbränslehantering AB.

**Cvetkovic V, 2010.** Significance of fracture rim zone heterogeneity for tracer transport in crystalline rock. Water Resources Research 46, W03504. doi:10.1029/2009WR007755

**Eklund S, Mattsson K-J, 2009.** Forsmark site investigation. Quantitative mapping of fracture minerals in Forsmark. SKB P-08-47, Svensk Kärnbränslehantering AB.

**Fenter P, Geissbühler P, DiMasi E, Srajer G, Sorensen L B, Sturchio N C, 2000.** Surface speciation of calcite observed in situ by high-resolution X-ray reflectivity. Geochimica et Cosmochimica Acta 64, 1221–1228.

**Haggerty R, 1999.** Application of the multirate diffusion approach in tracer test studies at Äspö HRL. SKB R-99-62, Svensk Kärnbränslehantering AB.

**Kelokaski M, Oila E, Siitari-Kauppi M, 2001.** Äspö Hard Rock Laboratory. TRUE Block Scale project. Investigation of porosity and microfracturing in granitic fracture wall rock and fault breccia specimens using the PMMA technique. SKB IPR-01-27, Svensk Kärnbränslehantering AB.

**Kuva J (ed), Myllys M, Timonen J, Kelokaski M, Ikonen J, Siitari-Kauppi M, Lindberg A, Aaltonen I, 2012.** Microstructure, porosity and mineralogy around fractures in Olkiluoto bedrock. Posiva 2012-02, Posiva Oy, Finland.

**Löfgren M, Sidborn M, 2010.** Statistical analysis of results from the quantitative mapping of fracture minerals in Forsmark. Site descriptive modelling – complementary studies. SKB R-09-30, Svensk Kärnbränslehantering AB.

**Möri A, Mazurek M, Adler M, Schild M, Siegesmund S, Vollbrecht A, Ota K, Ando T, Alexander W R, Smith P A, Haag P, Bühler C, 2003.** Grimsel Test Site. Investigation Phase IV (1994–1996). The Nagra–JNC in situ study of safety relevant radionuclide retardation in fractured crystalline rock. IV: The in situ study of matrix porosity in the vicinity of a water conducting fracture. Nagra Technical Report 00-08, Nagra, Switzerland.

**Nilsson K, Byegård J, Selnert E, Widestrand H, Höglund S, Gustafsson E, 2010.** Äspö Hard Rock Laboratory. Long Term Sorption Diffusion Experiment (LTDE-SD). Results from rock sample analyses and modelling. SKB R-10-68, Svensk Kärnbränslehantering AB.

**Painter S, Mancillas J, 2009.** MARFA version 3.2.2 user's manual: migration analysis of radionuclides in the far field. SKB R-09-56, Svensk Kärnbränslehantering AB.

**Painter S, Mancillas J, 2013.** MARFA user's manual: migration analysis of radionuclides in the far field. Posiva Working Report 2013-01, Posiva Oy, Finland.

**Parkhomenko E I, 1967.** Electrical properties of rocks. New York. (Monographs in geoscience)

**Penttinen L, Siitari-Kauppi M, Ikonen J, 2006a.** Forsmark site investigation. Determination of porosity and micro fracturing using the $^{14}$C-PMMA technique in samples taken from Forsmark area. SKB P-06-60, Svensk Kärnbränslehantering AB.

**Penttinen L, Siitari-Kauppi M, Ikonen J, 2006b.** Oskarshamn site investigation. Determination of porosity and micro fracturing using the $^{14}$C-PMMA technique in samples taken from Oskarshamn area. SKB P-06-62, Svensk Kärnbränslehantering AB.

**Petersson J, Wängnerud A, Stråhle A, 2003.** Forsmark site investigation. Boremap mapping of telescopic drilled borehole KFM02A. SKB P-03-98, Svensk Kärnbränslehantering AB.

**Posiva, 2013.** Safety case for the disposal of spent nuclear fuel at Olkiluoto – Models and data for the repository system 2012. Posiva 2013-01, Posiva Oy, Finland.

**Rouhiainen P, Pöllänen J, 2004.** Forsmark site investigation. Difference flow logging in borehole KFM02A. SKB P-04-188, Svensk Kärnbränslehantering AB.

**Selnert E, Byegård J, Widestrand H, 2008.** Forsmark site investigation. Laboratory measurements within the site investigation programme for the transport properties of the rock. Final report. SKB P-07-139, Svensk Kärnbränslehantering AB.

**Selroos J-O, Painter S L, 2012.** Effect of transport-pathway simplifications on projected releases of radionuclides from a nuclear waste repository (Sweden). Hydrogeology Journal 20, 1467–1481.

**Siitari-Kauppi M, Ikonen J, Kauppi L, Lindberg A, 2010.** Investigation of porosity and pore structure adjacent to fractures by PMMA method; samples taken from drill cores at Olkiluoto. Posiva Working Report 2010-66, Posiva Oy, Finland.

**SKB, 2004.** RETROCK Project. Treatment of geosphere retention phenomena in safety assessments. Scientific basis of retention processes and their implementation in safety assessment models (WP2). Work package 2 report of the RETROCK concerted action. SKB R-04-48, Svensk Kärnbränslehantering AB.

**SKB, 2010a.** Radionuclide transport report for the safety assessment SR-Site. SKB TR-10-50, Svensk Kärnbränslehantering AB.

**SKB, 2010b.** Geosphere process report for the safety assessment SR-Site. SKB TR-10-48, Svensk Kärnbränslehantering AB.

**SKB, 2010c.** Data report for the safety assessment SR-Site. SKB TR-10-52, Svensk Kärnbränslehantering AB.

**SKB, 2011.** Long-term safety for the final repository for spent nuclear fuel at Forsmark. Main report of the SR-Site project. SKB TR-11-01, Svensk Kärnbränslehantering AB.

**Stephens M B, Fox A, La Pointe P R, Simeonov A, Isaksson H, Hermanson J, Öhman J, 2007.** Geology Forsmark. Site descriptive modelling Forsmark stage 2.2. SKB R-07-45, Svensk Kärnbränslehantering AB.

**Vieno T, Nordman H, 1999.** Safety assessment of spent fuel disposal in Hästholmen, Kivetty, Olkiluoto and Romuvaara − TILA-99. Posiva 99-07, Posiva Oy, Finland.

**Vilks P, Miller N H, Stanchell F W, 2004.** Phase II in-situ diffusion experiment. Report 06819-REP-01200-10128-R00, Ontario Power Generation, Nuclear Waste Management Division, Canada.

**Vilks P, Miller N H, Stanchell F W, 2005.** Laboratory program supporting SKB's long term diffusion experiment. Report 06819-REP-01300-10111-R00, Ontario Power Generation, Nuclear Waste Management Division, Canada.

**Widestrand H, Byegård J, Cvetkovic V, Tullborg E-L, Winberg A, Andersson P, Siitari-Kauppi M, 2007.** Sorbing tracer experiments in a crystalline rock fracture at Äspö (Sweden): 1. Experimental setup and microscale characterization of retention properties, Water Resources Research 43, W10413. doi:10.1029/2006WR005277

**Widestrand H, Byegård J, Selnert E, Skålberg M, Höglund S, Gustafsson E, 2010.** Long term sorption diffusion experiment (LTDE-SD). Supporting laboratory program – Sorption diffusion experiments and rock material characterization. With supplement of adsorption studies on intact rock samples from the Forsmark and Laxemar site investigations. SKB R-10-66, Svensk Kärnbränslehantering AB.

**Winberg A, Andersson P, Byegård J, Poteri A, Cvetkovic V, Dershowitz W, Doe T, Hermanson J, Gómez-Hernández J J, Hautojärvi A, Billaux D, Tullborg E-L, Holton D, Meier P, Medina A, 2003.** Final report of the TRUE Block Scale project. 4. Synthesis of flow, transport and retention in the block scale. SKB TR-02-16, Svensk Kärnbränslehantering AB.

**Zhou Q, Liu H-H, Molz F J, Zhang Y, Bodvarsson G S, 2007.** Field-scale effective matrix diffusion coefficient for fractured rock: results from literature survey. Journal of Contaminant Hydrology 93, 161–187

# Appendix 1 – Magnification of central case study results

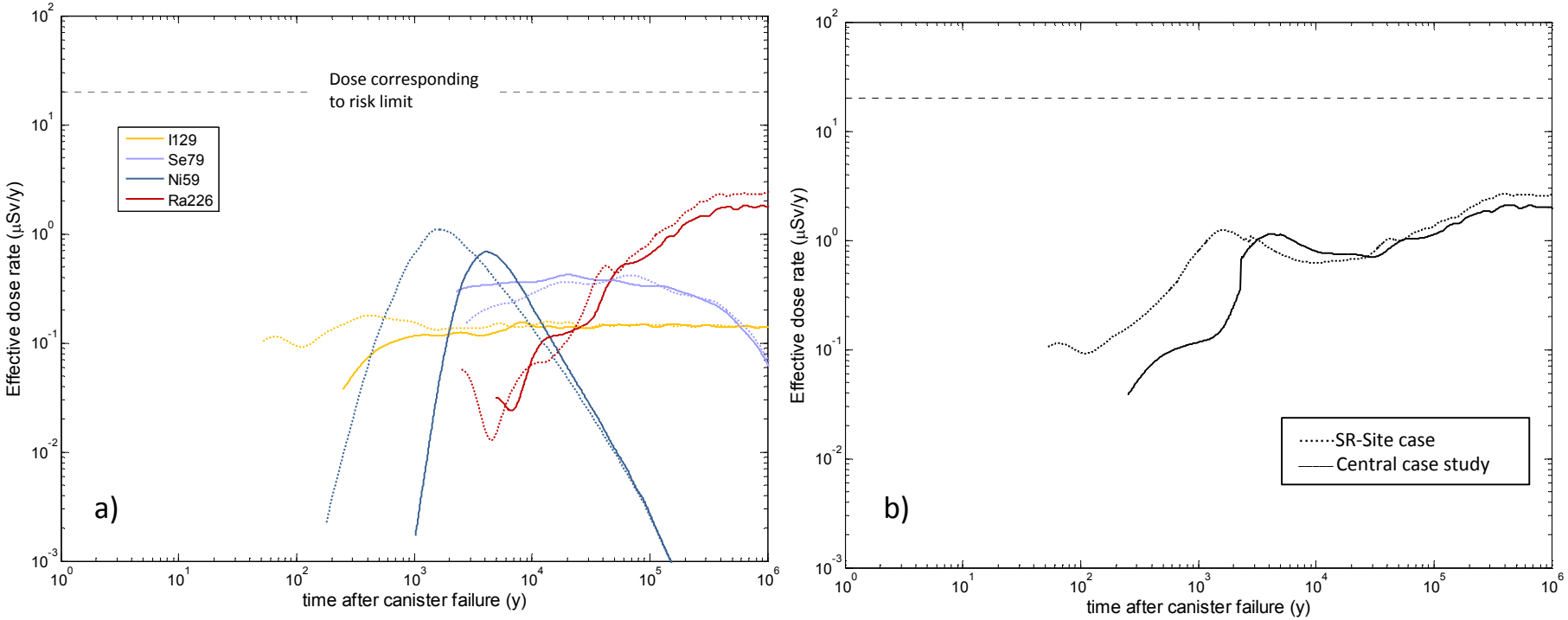


*Far-field dose rate results for central case study, flowpath 1. Breakthrough curves for the SR-Site case of undisturbed rock matrix shown as broken lines; central case study shown as solid lines. Left panel shows individual nuclide contributions to dose; right panel shows total summed dose for modelled nuclides.*

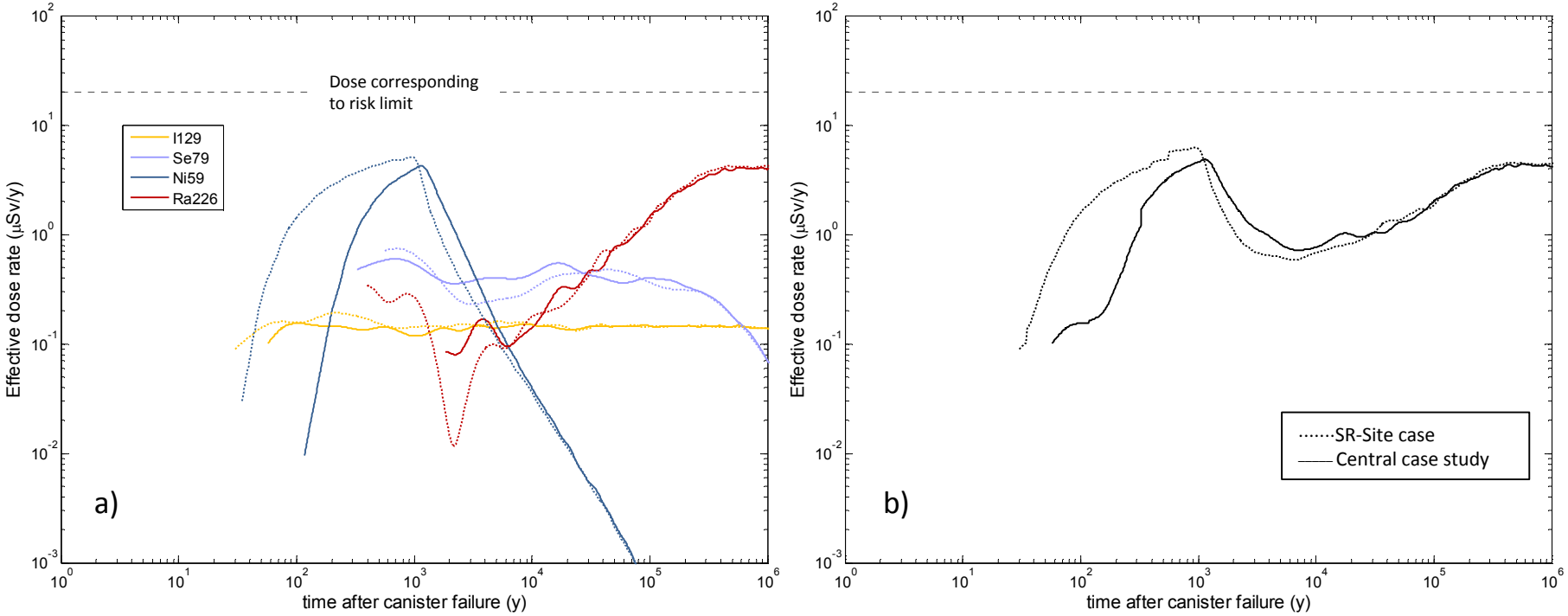


*Far-field dose rate results for central case study, flowpath 2. Breakthrough curves for the SR-Site case of undisturbed rock matrix shown as broken lines; central case study shown as solid lines. Left panel shows individual nuclide contributions to dose; right panel shows total summed dose for modelled nuclides.*

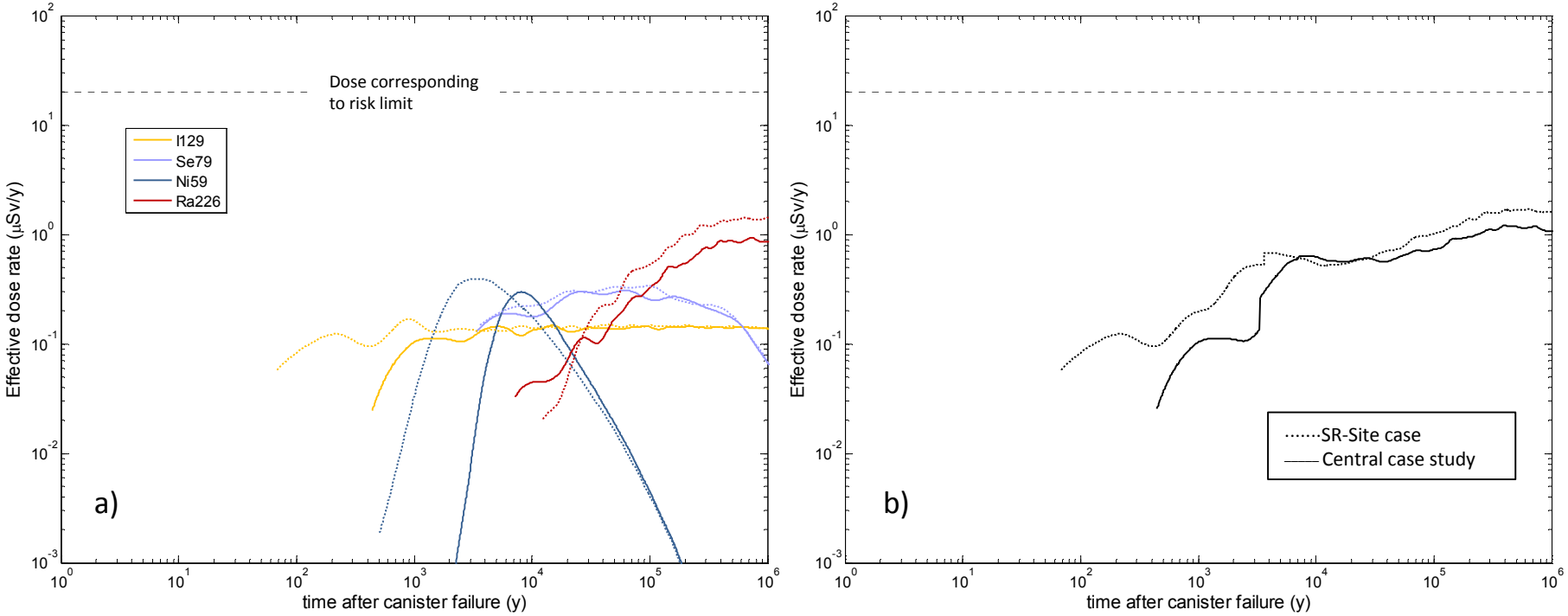


*Far-field dose rate results for central case study flowpath 3. Breakthrough curves for the SR-Site case of undisturbed rock matrix shown as broken lines; central case study shown as solid lines. Left panel shows individual nuclide contributions to dose; right panel shows total summed dose for modelled nuclides.*

# Appendix 2 – Parameterisation of the layered rock model

In Figure 5, the layered rock model of the central case study is provided, featuring 11 different layers in total. The parameters used to describe each of these layers are the thickness, the porosity, the effective diffusivity, and the anion exclusion factor. Except for these parameters, the additional parameter provided is the surface portion that is needed for estimating the fracture class specific F-factor. It should be kept in mind that there exist very little site specific data for the fracture coatings and alteration rim, in terms of porosities and effective diffusivities, and that some of the estimates discussed in this appendix are merely educated guesses.

### Surface portion – general considerations

Concerning the immediate far field we have chosen to base the different surface portions of the fracture classes on the distribution of different fracture minerals in the fracture coating layer. By doing this, we effectively disregard that the parameter values of all layers may differ between fracture classes. The rational is that there exist a large body of empirical data on the spatial distribution of fracture minerals, and that there is a lack of site specific knowledge on how altered rock of different characteristics is distributed. With current site specific knowledge, we cannot predict what type of altered rock is likely to be associated with a specific fracture coating layer. As a result, this gap in knowledge must be handled by varying the altered rock properties in the variant case modelling, or by assuming pessimistic values. Concerning undisturbed rock, the large body of data available (e.g. Selnert et al. 2008, Crawford 2008, SKB 2010c) suggests that different rock volumes of undisturbed rock have fairly similar matrix diffusion properties. Consequently, it is reasonable to use the same parameterisation of the undisturbed rock layers for all fracture classes. For this reason, the undisturbed rock has not been considered in assigning the surface portion of the fracture classes.

Judging from existing knowledge of fracture surfaces, including site specific knowledge from inspecting drill core surfaces facing natural open fractures (Eklund and Mattsson 2009), fracture minerals often cover small patches of the fracture surface. Furthermore, site specific evidence suggests that part of the fracture surfaces is uncovered. This would suggest that even on the scale of the drill core cross section area (~0.002 $m^2$), different parts could conform to different fracture classes. To acknowledge this small-scale heterogeneity when estimating the surface portion, the chosen approach is to sum all fracture surface areas conforming to a fracture class, irrespectively of how small the areas of the individual patches are. From the perspective of solute transport modelling, where flowpath averaging of fracture properties are performed in one way or another, one is interested in the portions of the flowpath having different retention properties. As long as rock volumes on a larger scale feature a similar pattern of fracture minerals, the local sequence of fracture classes would be of limited importance. By analysing the distribution of the most important fracture minerals at Forsmark it was concluded that there is no great difference in fracture mineral occurrence between large-scale rock volumes (Löfgren and Sidborn 2010). Consequently, the approach of summing all surfaces conforming to a fracture class is judged as suitable for providing input data to solute transport modelling.

In a special site specific campaign of mapping drill cores, the quantitative surface coverage and thickness of the most common fracture minerals have been investigated (Eklund and Mattsson 2009, Löfgren and Sidborn 2010). The campaign was much

focused on local rock volumes where groundwater flow had been detected by the Posiva difference flow meter in the site investigation. One meter of drill core on each side of 401 flow anomalies (so called PFL-anomalies) were investigated and the fracture minerals of 2,071 open fractures were mapped. For each fracture, up to eight layers of fracture minerals, four for each of the fracture surface, were recorded. Not all fracture minerals were mapped, but only the once judged to have the greatest impact on solute transport and reaction. These minerals were calcite, chlorite, clay minerals (as a group), hematite, and pyrite. In addition, hematite staining as well as occurrences of uncoated, seemingly fresh wall rock were recorded.

In the following, the mapping methodology concerning the total coverage is shortly described. If the reader has problems understanding this short description, it is recommended to review the full description of the mapping campaign provided in Löfgren and Sidborn (2010). The total coverage represents the percentage of the drill core fracture surface that an individual fracture mineral layer covers. Figure 14 illustrates a drill core sample where the rock matrix is over-layered by three different fracture mineral layers facing a natural fracture surface. The individual layers do not have to cover the entire surface, and do not have to have a uniform thickness (as demonstrated by layer A).

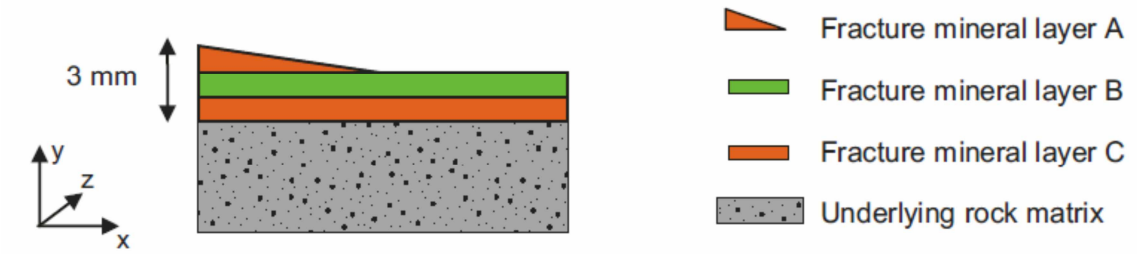


***Figure 14.*** *Illustration of a rock sample covered by three layers of fracture minerals. Reproduced from Löfgren and Sidborn (2010, Figure 2-3).*

The total coverage of each layer is estimated based on ocular inspection of the layer occurrence at the perimeter of the drill core sample, as well as by ocular inspection of the drill core sample surface. If, for simplicity, assuming that the layers in Figure 14 are constant in the z-axis, layers B and C have a total coverage of 100%, while layer A has a total coverage of 50%. The total coverage is estimated for up to four different layers for both the upper and lower fracture surface of the drill core. As it turns out the situation in Figure 14, indicating that at least one layer covers 100% of the fracture surface, is not the most common. The common situation appears to be that part of the fracture surface is uncovered by any fracture mineral, also on the scale of the drill core sample cross section area.

By using raw data[7] from the mapping campaign described in Eklund and Mattsson (2009) and Löfgren and Sidborn (2010) it can be determined, on average, what percentage of the fracture surface is uncovered (fracture class 1:2), covered by calcite (fracture class 1:3) or by chlorite and clay minerals (fracture class 1:1). In Löfgren and Sidborn (2010), fracture mapping data were sorted into different elevation ranges, where the one of most interest for the immediate far field would be elevation range 300–500 mbsl (metres below sea level). However, when treating raw data in this present report, data from the entire elevation range, that is from ground surface to the end of borehole (up to 1,000 m deep), have been used.

[7] Data delivery note Sicada_08_090

### Surface portion – fracture class 1:2

The surface portion reflects the portion of the flowpath's total surface that is constituted by the individual fracture class. Concerning fracture class 1:2, both the upper and lower fracture surfaces of the drill core were found to be totally uncoated for 18% of all investigated fractures in the entire elevation range, and for 25% of all investigated fractures in the elevation range 300–500 mbsl (Löfgren and Sidborn 2010, Table 3-16). As the immediate far field is located in the elevation range 300–500 mbsl, fracture class 1:2 should at least constitute 25% of the flowpath length. However, as argued for above, one needs to add the contribution from drill core surfaces that are only partly uncoated. This was not done in Löfgren and Sidborn (2010) and, accordingly, the raw data obtained in the mapping campaign have been revisited. By inspecting the raw data it was found that in an overwhelming majority of the cases, underlying fracture minerals had a higher total coverage than overlying fracture minerals. This can be exemplified by layers A and B in Figure 14, where the overlaying layer A has the total coverage of 50% while the underlying layer B as the larger total coverage of 100%. Based on this knowledge, a simplification was made to assume that layers are stacked on top of each other. Importantly, the simplification was made that no layer of minor total coverage exists side by side with the layer of the highest total coverage (cf. Figure 15). The total fraction of uncovered rock is then taken as 100% minus the total coverage of the layer, out of the possible four, having the maximum total coverage. With this simplification, the upper boundary for the uncovered surface area can be explored.

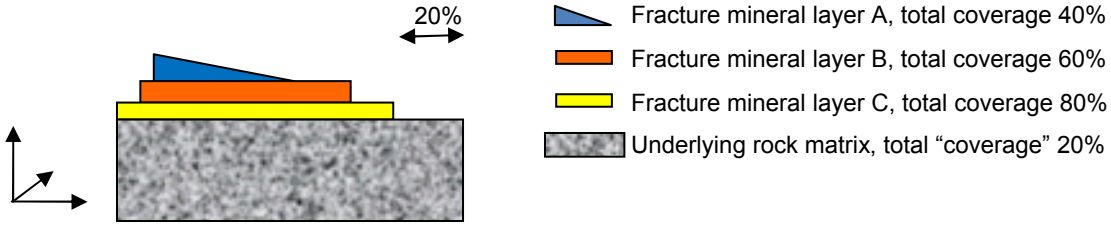


***Figure 15.*** *Illustration of a rock sample covered by three layers of fracture minerals that are stacked on each other, not existing side by side, revealing an uncovered surface of 20%.*

In Figure 16 a cumulative distribution function (CDF) of the total coverage of the one layer having the maximum total coverage per fracture surface is provided, including data from the 2,071 open fractures mapped in Eklund and Mattsson (2009).

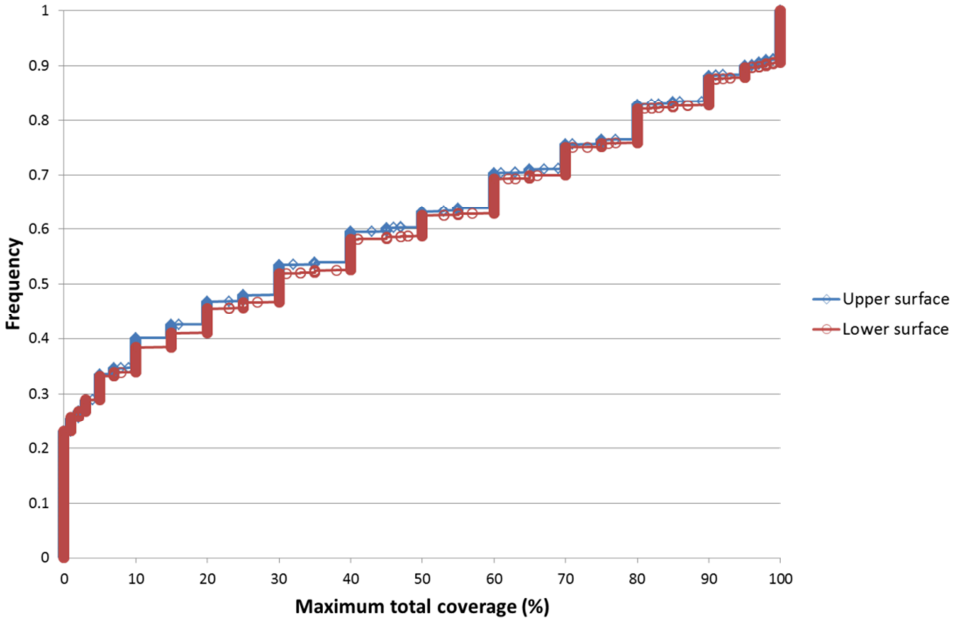


***Figure 16.*** *CDF of the total coverage of the fracture mineral layer having the maximum value per fracture surface. Blue data signify the upper fracture surface while red data signify the lower fracture surface.*

If studying Figure 16 one can see that only about 10% of both fracture surfaces have, at least, one layer covering the entire surface. For 23% of the upper fracture surfaces, as well as of the lower fracture surfaces, no fracture mineral covers the wall rock. On average (arithmetic mean), the layer having the maximum total coverage per fracture surface covers about 39% of the drill core cross section area. This sets the upper boundary for the coverage of fresh wall rock to, on average, 61%. Except for the requirement that layers are stacked and do not exist side by side, there is also the requirement that fracture minerals that were not mapped in the campaign pose no significant interference with the result. For the central case study, it is judged that the figure 61% well enough represents the portion of the fracture surface that is uncoated, although the figure is rounded to 60%.

### Surface portion – fracture class 1:3

The fracture mineral calcite is assumed to coat the fracture surface of fracture class 1:3. Although calcite is one of the fracture minerals treated in Löfgren and Sidborn (2010), that report does not provide the data on the total coverage that we need. Consequently, we are forced to revisit the raw data[8] from the 2,071 open fractures mapped in (Eklund and Mattsson (2009). In Table 3, average data for the (up to) eight individually recorded fracture mineral layer of the mapping campaign are provided. The column "Population fraction" refers to the percentages of all 2,071 fractures that feature the specific fracture mineral in the specific layer. The column "Mean total coverage" is obtained by pooling the total coverages for the specific fracture mineral in the specific layer and by taking the arithmetic mean. The column "Mean layer thickness" reflects the thickness of the fracture mineral layer and is explained in detail later in this appendix.

[8] Data delivery note Sicada_08_090

**Table 3. Arithmetic mean of total coverage and thickness of the (up to) eight layers of fracture minerals recorded for each open fracture. Data for chlorite, clay minerals and calcite are based on all 2,071 fractures mapped in Eklund and Mattsson (2009).**

| | **Upper layer 1** | | | **Upper layer 2** | | |
|---|---|---|---|---|---|---|
| | Population fraction | Mean total coverage | Mean layer thickness[1] | Population fraction | Mean total coverage | Mean layer thickness |
| Chlorite | 11 % | 49 % | 0.07 mm | 26 % | 51 % | 0.11 mm |
| Clay minerals | 17 % | 42 % | 0.07 mm | 3 % | 40 % | 0.07 mm |
| Calcite | 38% | 21% | 0.11 mm | 11% | 27 % | 0.12 mm |
| | **Upper layer 3** | | | **Upper layer 4** | | |
| | Population fraction | Mean total coverage | Mean layer thickness | Population fraction | Mean total coverage | Mean layer thickness |
| Chlorite | 9 % | 62 % | 0.09 mm | 1 % | 74 % | 0.12 mm |
| Clay minerals | 0.3 % | 39 % | 0.08 mm | 0 % | - | - |
| Calcite | 1% | 42 % | 0.16 mm | 0.1 % | 23 % | 0.08 mm |
| | **Lower layer 1** | | | **Lower layer 2** | | |
| | Population fraction | Mean total coverage | Mean layer thickness | Population fraction | Mean total coverage | Mean layer thickness |
| Chlorite | 12 % | 50 % | 0.08 mm | 24 % | 55 % | 0.10 mm |
| Clay minerals | 18 % | 45 % | 0.08 mm | 3 % | 44 % | 0.08 mm |
| Calcite | 33% | 21% | 0.10 mm | 11% | 22 % | 0.14 mm |
| | **Lower layer 3** | | | **Lower layer 4** | | |
| | Population fraction | Mean total coverage | Mean layer thickness | Population fraction | Mean total coverage | Mean layer thickness |
| Chlorite | 8 % | 62 % | 0.09 mm | 1 % | 67 % | 0.09 mm |
| Clay minerals | 0.3 % | 62 % | 0.11 mm | 0 % | - | - |
| Calcite | 1% | 38 % | 0.23 mm | 0.1 % | 25 % | 0.10 mm |

[1] For all individual mineral layers, when a mineral coverage is noted but its thickness is below detection limit (0.1 mm), the thickness 0.05 mm is assigned (half of the detection limit).

As one can see in Table 3, calcite was found as the layer directly facing the fracture (layer 1) in 38% and 33% of the cases for the upper and lower fracture surface, respectively. In layer 2, calcite was found in 11% of the cases for both the upper and lower fracture surfaces. Concerning layers 3 and 4, calcite was only found in 1% of the cases, or less. Accordingly these two layers have been neglected when processing the data.

The same fracture mineral cannot exist in two adjacent layers on the same fracture surface. They would then have been reported as a single layer of larger thickness. To exemplify, one can be sure that drill core samples having calcite in upper layer 1 are different from those having calcite in upper layer 2. Therefore, when estimating the total coverage of calcite along the flowpath, one can add the contribution from layers 1 and 2. Hence, the total coverage of the flowpath, conforming to fracture class 1:3, can be calculated as following.

- Total coverage of flowpath = $\Sigma$ (population fraction $\cdot$ total coverage)/2
  $(38\% \cdot 21\% + 11\% \cdot 27\% + 33\% \cdot 21\% + 11\% \cdot 22\%) / 2 = 10\%$

In the above calculation, four products are summed relating to upper layers 1 and 2 and lower layers 1 and 2. The first value of the first product (38%) is the population fraction

the upper layer 1 of Table 3, while the second value of the product (21%) is the mean total coverage of upper layer 1. The remaining three products relate to the other layers. The sum is divided by two; to account for the fact that both fracture surfaces have been used in the calculation. This resulting value, 10%, means that calcite surrounds the flowpath for 10 percent of the entire contact area between the flowpath and surrounding rock (the so called flow-wetted surface). Although the raw data come from rock volumes that would include both the immediate far field and the distant far field, it is judged that the value 10% is suitable for the surface portion of fracture class 1:3. This is based on the conclusion in Löfgren and Sidborn (2010) that there are relatively small differences in fracture mineral occurrences in different rock volumes at Forsmark.

### Surface portion – fracture class 1:1

Fracture class 1:1 is covered by a fracture coating assumed to consist of chlorite and/or clay minerals. For clay minerals, as for calcite discussed above, occurrences are found in mineral layer 1 and 2, but occurrences in layer 3 and 4 are sparse or even non-existing (cf. Table 3). Accordingly, we can calculate the "Total coverage of flowpath" for clay minerals by using the same approach as for calcite:

- Total coverage of flowpath, clay minerals $= \Sigma$ (population fraction · total coverage)/2 = (17% · 42% + 3% · 40% + 18% · 45% + 3% · 44%) / 2 = 9%

For chlorite it turns out that significant occurrences are also noted in mineral layer 3, in addition to occurrences in layers 1 and 2 (cf. Table 3). However, for unknown reasons, there is no logged occurrence of chlorite in both layer 1 and 3. Furthermore, based on the reasoning above on occurrences of the same mineral in adjacent layers, chlorite cannot occur in both mineral layer 1 and 2, or in 2 and 3, for the same fracture surface. As a result, we can calculate the "Total coverage of flowpath" for chlorite in an analogue way as for calcite and clay minerals, but internalising data for the first three layers in Table 3.

- Total coverage of flowpath, chlorite $= \Sigma$ (population fraction · total coverage)/2 = (11% · 49% + 26% · 51% + 9% · 62% + 12% · 50% + 24% · 55% + 8% · 62%) / 2 = 24%

The raw data, and the mapping methodology, leaves no room of combining the "Total coverage of flowpath" for clay minerals and chlorite in a rigorous way. It can only be said that the combined value should be within the range 24% and 33% (24% + 9%). Based on this, the round figure 30% is chosen for the surface portion of fracture class 1:1. This is also in agreement with the surface portions of fracture class 1:2 (60%) and 1:3 (10%), as the three surface portions add up to 100%.

### Surface portion – fracture class 2:1

In the distant far field, fracture class 2:1 is assumed to constitute the entire flowpath. Accordingly, its surface portion is 100%.

### Fracture coating thickness – general considerations

In the special campaign of mapping fracture minerals, discussed above, the layer thickness was estimated for each individual fracture mineral layer. This was done by ocular inspection of the drill core sample, mainly at its perimeter, and by averaging the layer thickness of five readings (if possible). By the methodology used (Löfgren and Sidborn 2010, Section 2.1.2), the layer thickness should be seen as the mean thickness of the layer where it covers the fracture surface. If revisiting Figure 14 and in this instance make the simplifying assumption that the sample is a slab of constant

properties in the z-axis, the layer thickness of layer A is 0.5 mm. Here 0.5 mm is the average thickness of the right-angled triangle with the height 1 mm, regardless of the fact that layer A only covers 50% of the fracture surface.

In Table 3, the column "Mean layer thickness" is obtained by pooling the layer thicknesses for the specific fracture mineral in the specific layer and by taking the arithmetic mean. On many occasions, it is noted that there exist a fracture mineral layer, having a certain total coverage, but where the layer thickness is below the detection limit of 0.1 mm. In such cases, a layer thickness of 0.05 mm, which is half of the detection limit, has been assumed in this report.

The bounding value for the maximum total thickness of the fracture coating can be obtained by summing the layer thicknesses of the, up to, eight individual layers associated with an open fracture. A prerequisite for doing this is that fracture minerals not studied in the mapping campaign will not add significantly to the thickness of the fracture coating. It is judged that this is a reasonable assumption. In Figure 17, this bounding value for the 2,071 mapped fractures is displayed as a cumulative distribution function (CDF).

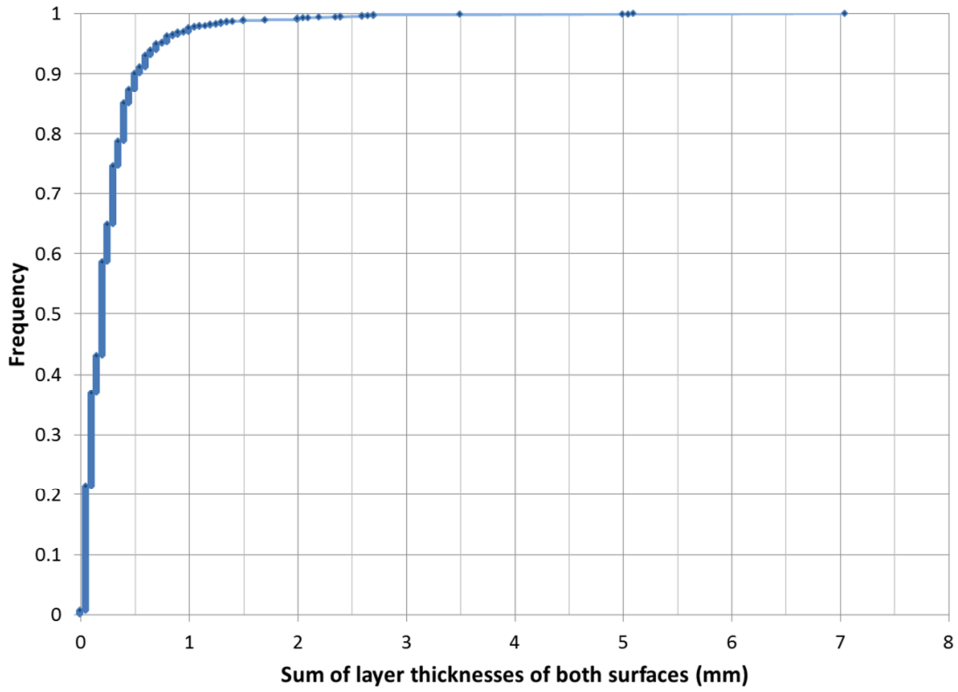


*Figure 17. CDF of the maximum total thickness of the fracture coating which is the sum of the layer thicknesses for the, up to, eight fracture mineral layers of each mapped fracture. To obtain the maximum total thickness of the fracture coating for each of the fracture surfaces, the data should be divided by two.*

By this approach the thicknesses of layers that may only cover a small part of the fracture surface are internalised in the sum. Accordingly, the average thickness of the fracture coating would only correspond to the maximum total thickness if all layers had total coverages of 100%, which is not the observed case. In the general case, the average thickness of the fracture coating would be smaller than the corresponding data point shown in Figure 17. For this reason, the data in Figure 17 are only used for comparative purposes for the immediate far field. They could also be used for assigning bounding values when modelling variant cases.

Below, the assumed fracture coating thicknesses of the different fracture classes are presented, for the central case study. It should once more be noted that the fracture coating thicknesses correspond to the patches where the fracture mineral exist. The fact that the specific layer does not cover the entire fracture surface is already internalised in the definition of the fracture classes' surface portion.

### Fracture coating thickness – fracture class 1:3

The fracture mineral calcite coats fracture class 1:3. Once more we use the fact that calcite is frequently occurring in layers 1 and 2 (cf. Table 3) but is very sparsely occurring in layers 3 and 4, and disregard the latter layers. As the same fracture mineral cannot exist in two adjacent layers, the occurrences in layer 1 and 2 must correspond to different fractures. As can be seen from Table 3, the mean layer thickness for calcite in upper and lower layers 1 and 2 ranges from 0.10 to 0.14 mm. If weighting the four values based on the corresponding population fraction one gets:

- Fracture coating thickness = (38% · 0.11 mm + 11% · 0.12 mm + 33% · 0.10 mm + 11% · 0.14 mm) / 98% = 0.11 mm

In the above calculation, four products are summed relating to upper layers 1 and 2 and lower layers 1 and 2. The first value of the first product (38%) is the population fraction the upper layer 1 of Table 3, while the second value of the product (0.11 mm) is the mean layer thickness of upper layer 1. The remaining three products relate to the other layers. The sum of the products is divided by the sum of the four layers' population fractions (98%). This is as one should disregard the fact that the patches of fracture minerals of interest do not cover the entire fracture surface. As stated previously, this fact is already internalised when assigning the surface portion. The result 0.11 mm is used when assigning data to the central case study for the fracture coating thickness of fracture class 1:3. However, it is rounded to 0.1 mm. This fracture coating thickness can be compared with the corresponding data for the TURVA-2012 safety case, for the calcite-coated transport class, where a layer thickness of 0.2 mm was assigned (Posiva 2013, Table 7-14).

### Fracture coating thickness – fracture class 1:1

The same arithmetic operation can be done for clay minerals and chlorite, as for calcite. Using data from Table 3 one would get:

- Fracture mineral thickness – clay minerals = (17% · 0.07 mm + 3% · 0.07 mm + 18% · 0.08 mm + 3% · 0.08 mm) / 41% = 0.08 mm
- Fracture mineral thicknesses – chlorite = (11% · 0.07 mm + 26% · 0.11 mm + 9% · 0.09 mm + 12% · 0.08 mm + 24% · 0.10 mm + 8% · 0.09 mm) / 90% = 0.09 mm

This means that for both fracture minerals, the fracture mineral thickness is, on average, a little below 0.1 mm. Again the raw data, and the mapping methodology, leaves no room of combining the thicknesses for clay minerals and chlorite in a rigorous way. One way of combining the data would be to sum 0.08 and 0.09 mm, resulting in a fracture coating thickness of 0.17 mm. However, this may lead to an overestimation of the combined thickness, as the two fracture minerals may not exist in the same fracture in each case, and if they do, need not to have the corresponding total coverages. Therefore, the fracture coating thickness of 0.17 mm can be seen as an upper bounding value. A second way of combining the data would to take the average between the lower bounding value (0.08 mm) and the upper bounding value, resulting in 0.13 mm. These

two values can be compared with the data in the cumulative distribution function of the maximum total thickness of the fracture coating in Figure 17. At CDF = 50%, the maximum total thickness of the fracture coating is 0.2 mm for both fracture surfaces. Accordingly, the value 0.1 mm is reasonable for a single fracture surface. Fracture class 1:1 is intended to correspond to the general perception of the rock that surrounds discrete fractures in sparsely fractured crystalline rock. Therefore, it would be inappropriate to assign a fracture coating thickness that is larger than the median value of Figure 17. Consequently, the fracture coating thickness of fracture class 1:1 is set to be 0.1 mm. This fracture coating thicknesses can be compared with the corresponding data for the TURVA-2012 safety case, for the clay-coated transport class, where a layer thickness of 0.2 mm was assigned (Posiva 2013, Table 7-13).

### Fracture coating thickness – fracture class 2:1

No specific fracture mineral is assigned to the fracture coating of fracture class 2:1. It is assumed that fracture class 2:1 corresponds to a major fracture zone, and that it resembles the fractures investigated in the TRUE series of experiments at the Äspö Hard Rock Laboratory. Accordingly, it is assumed that the wall rock is covered by a relatively thick fracture coating. If studying Figure 17 one can see that when CDF = 99 %, the fracture coating thickness (for each of the fracture surfaces) corresponds to 1 mm. This value is chosen for the fracture coating thickness of fracture class 2:1.

### Fracture coating porosity and effective diffusivity – general considerations

Very few site specific data exist on the porosity of fracture coatings, from sealed fractures, while no site specific effective diffusivity data exists. Furthermore, in a limited literature study, no reliable data of the effective diffusivity of fracture minerals has been found, as relevant for the geological conditions at Forsmark. For this reason, porosity data from the Forsmark, Oskarshamn and Oilkiluoto sites, as generally obtained from $^{14}$C-PMMA impregnations, have been used. Based on these data, together with more or less reliable relations between the porosity and effective diffusivity, educated guesses have been made to assign effective diffusivities to the fracture mineral layers.

In the Finnish safety case TURVA-2012, porosities and effective diffusivities were assigned to fracture coating layers of different transport classes. For the clay-coated transport class, as well as for the calcite-coated transport class, the porosity of 6% and effective diffusivity of $1 \cdot 10^{-12}$ m$^2$/s were assigned (Posiva 2013, Tables 7-13 and 7-14). For the slickensided transport class, the porosity of 1% and effective diffusivity of $1 \cdot 10^{-13}$ m$^2$/s were assigned (Posiva 2013, Tables 7-15).

### Fracture coating porosity and effective diffusivity – fracture class 1:1

In Penttinen et al. (2006a, Section 4.7) a fracture adjacent sample from the Forsmark site was investigated by the $^{14}$C-PMMA impregnation method. For this sample it was found that there existed mineral bands with a porosity of over 5%, and that they seem to be chloritized biotite. For another fracture adjacent sample, that appeared to be more heavily altered, mineral grains with up to 20% porosity were detected, partly corresponding to sealed fractures (Penttinen et al. 2006a, Figures 4-24 to 4-27). The report also shows results from impregnations of other rock pieces from the Forsmark site, but either they lack sealed fracture or the wall rock is non-typical for the site.

In Penttinen et al. (2006b, Section 5.6) a fracture adjacent sample from the Oskarshamn site is discussed, featuring a thick “clayish” fracture coating with the PMMA porosity of

above 10%. In Penttinen et al. (2006b, Section 5.7) the porosity of the (unspecified) fracture filling material is estimated to be about 3–5%. In Penttinen et al. (2006b, Section 5.7) a rock sample is investigated having altered clay phases forming a connective network of highly porous veins with over 20% porosity. The report also shows results from impregnations of other rock pieces but the one summarised here are judged to be the ones with most bearing on the present problem of estimating the fracture coating porosity.

In Kuva et al. (2012, Section 3.2) the porosity of so called "clay fractures" were investigated by the $^{14}$C-PMMA impregnation method for rock samples from Oilkiluoto. The porosity of the sealed fractures varied but was on many occasions found to be on the order of 10%. This was also the general perception of Siitari-Kauppi et al. (2010).

In Widestrand et al. (2010, Appendix 3) a sample featuring sealed fractures was investigated by $^{14}$C-PMMA impregnation. Chlorite/epidote and/or calcite constituted the sealed fractures, showing high porosity in the autoradiographs, up to 30%.

Based on the above investigations, an educated guess was made for the porosity of the chlorite/clay minerals fracture coating of fracture class 1:1, of 10%. At such a high porosity, it is not unreasonable to use Archie's law (Archie 1942), which relates the formation factor $F_f$ (–) and the porosity $\varepsilon$ (–):

$$F_f = \varepsilon^m \qquad \text{Equation 2}$$

where $m$ is an empirical fitting parameter that is given between 1.8 and 2.0 for consolidated sandstone and as 1.3 for packed unconsolidated sand. Archie's law was modified by Parkhomenko (1967) to improve its applicability in crystalline rock.

$$F_f = 0.71\varepsilon^{1.58} \qquad \text{Equation 3}$$

However, for the dense and low-porous Forsmark rock matrix, the precision of Equation 3 has proven to be poor (e.g. Byegård et al. 2008, Figure 3-5). If arguing that relations for the rock matrix is poorly applicable for fracture coatings, it may be appropriate to use an empirical relation between the porosity and effective diffusivity of bentonite clay that was indirectly used in SR-Site. If combining Equations 5-1 and 5-4 in SKB (2010c) one gets:

$$D_e = 3.48 \cdot 10^{-9} e^{0.00205 \cdot \rho_s (\varepsilon - 1)} \qquad \text{Equation 4}$$

where $\rho_s$ (kg/m$^3$) is the density of the solid clay particle, which is taken to be 2,780 kg/m$^3$ (SKB 2010c, Section 5.1.1). This empirical relation is justified in the porosity range ~20% to ~80%, based on the dry density range shown in SKB (2010c, Figure 5-6).

In Figure 18, the effective diffusivity is plotted versus the porosity, based on the different relations shown in Equation 1 to Equation 4. When obtaining the effective diffusivity by using Archie's law, the value $D_w = 1 \cdot 10^{-9}$ m$^2$/s was used for the diffusivity in unconstrained pore water.

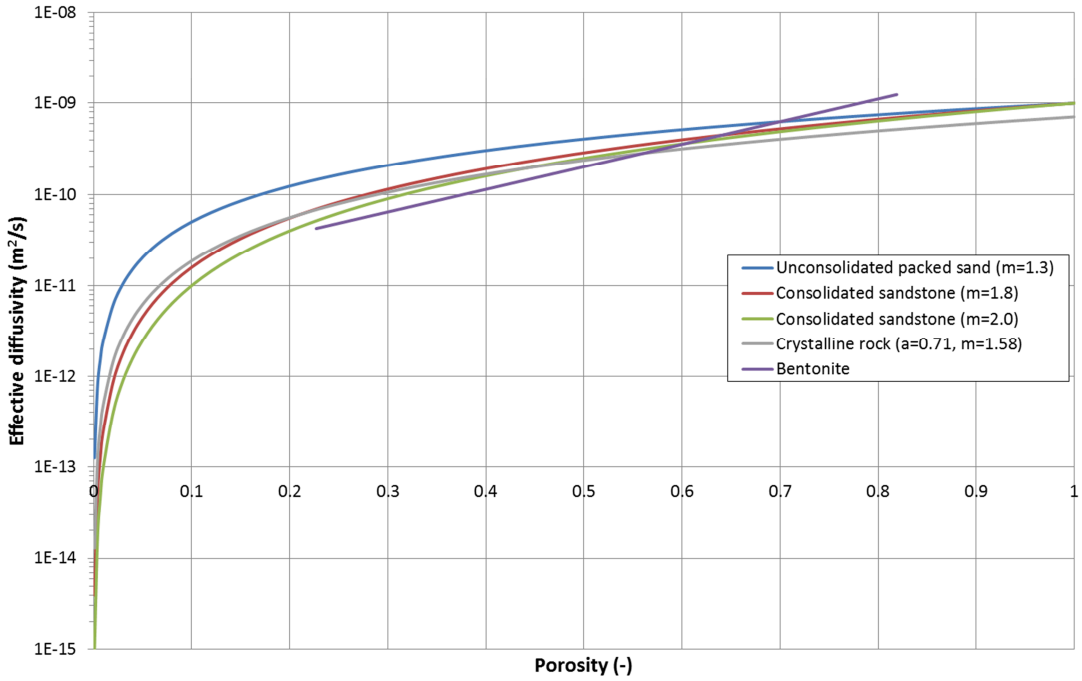


*Figure 18. Relations between the porosity and effective diffusivity. The first four relations are Archie's law with different fitting parameters. The fifth relation, labelled "Bentonite" corresponds to Equation 4.*

For a porosity of 10%, the combined information from the different relations suggests an effective diffusivity of just about $10^{-11}$ m$^2$/s. Consequently, for fracture class 1:1 the educated guess on the porosity and effective diffusivity is 10% and $2 \cdot 10^{-11}$ m$^2$/s.

### Fracture coating porosity and effective diffusivity – fracture class 1:3

Fracture class 1:3 features a fracture coating made up of calcite. For this fracture mineral, or for the group of carbonate fracture minerals, there are contradicting observations. In Siitari-Kauppi et al. (2010) sealed calcite fractures were on occasion found to be non-porous, or of very low porosity. The following conclusion was drawn:

> *"Fracture fillings were both highly porous and slightly or non porous; especially carbonate and calcite fillings were found to be low or non porous by the PMMA method. Calcite is known to be porous but it seems that the pores are isolated and not connecting to the open porosity network. In sample O7, a totally altered cordierite was non porous contrary to the cordierite grains normally observed in the studied samples."*

On other occasions calcite has been found to be highly porous, with a connected porosity (e.g. Widestrand et al. 2010, Appendix 3). By taking a pessimistic approach, it is assumed that the fracture coating of fracture class 1:3 has a high resistance to diffusion. This means that its porosity and effective diffusivity are assigned low values, even in comparison to the undisturbed rock matrix. There are no reliable data to support the assignment of specific values. Instead, it is merely assumed that the porosity and effective diffusivity is 0.1% and $1 \cdot 10^{-15}$ m$^2$/s, which is lower than for the undisturbed rock matrix.

### Fracture coating porosity and effective diffusivity – fracture class 2:1

The same porosity and effective diffusivity was assumed for the fracture coating of fracture class 2:1 as for fracture class 1:1, with a porosity of 10% and an effective diffusivity of $2 \cdot 10^{-11}$ $m^2/s$. The porosity equals that of the generalised conceptual model from the TRUE Block Scale project, shown in Figure 2, for the "very porous coating".

### Alteration rim thickness and porosity

In $^{14}$C-PMMA impregnations, (e.g. Penttinen et al. 2006a, b, Siitari-Kauppi et al. 2010, Widestrand et al. 2007, 2010), one can obtain the porosity distribution going from the fracture surface and into the rock matrix. The alteration rim can be seen as a zone of elevated porosity, where the porosity gradually declines towards the porosity of the undisturbed rock matrix, when moving away from the fracture. An example of such a result is provided in Figure 19, from a sample from the Oskarshamn site.

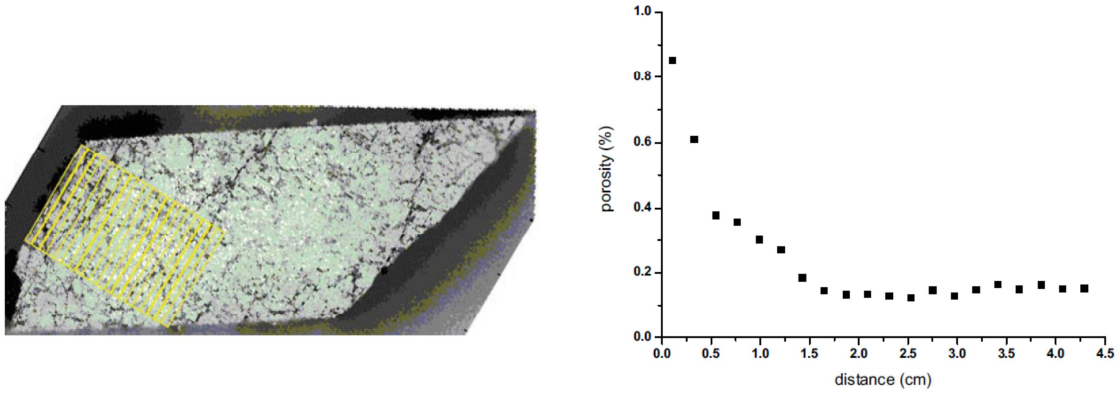


*Figure 19. $^{14}$C-PMMA porosity profile, relative to the fracture surface, for sample O11 from borehole KLX04. Reproduced from Penttinen et al. (2006b, Figure 5-40).*

Based on the general impression from reading reports on $^{14}$C-PMMA impregnations of rock types relevant for the Forsmark site, a typical alteration rim thickness appears to be on the order of 1 cm. This value is assigned to fracture class 1:1 and 1:3. For fracture class 1:2, featuring what is described as "fresh" rock surfaces, it has been assumed that the alteration is weak. A thickness of 0.5 cm, which is half the layer thickness of fracture class 1:1 and 1:3, is assigned to this fracture class. Fracture class 2:1 features a strong alteration rim with similarities to the generalised conceptual model from the TRUE Block Scale project, shown in Figure 2. In Figure 2, the alteration rim thickness appears to be on the order of 10 cm. This value, 10 cm, is adopted for fracture class 2:1.

Concerning the porosity of the alteration rim, the general impression from the above mentioned PMMA studies is that it on the order of 1%. On occasion, very high porosities are found in the first millimetre of the rock, but in these instances the porosity rapidly decreased at increased distances from the surface. In the layered rock model of Figure 5, three different porosity values are assigned to the alteration rims. The porosity of the moderate alteration rim of fracture class 1:1 and 1:3 is assumed to be 1%. The porosity of weakly altered rock in fracture class 1:2 is assumed to be 0.5% and that of the strongly altered rock in fracture class 2:1 is assumed to be 2%. Except for agreeing with the general impression of the alteration rim porosity range from PMMA impregnations, these values agree with the porosity limits given for altered wallrock in the generalised conceptual model from the True Block Scale project (cf. Figure 2). The adopted data are somewhat reduced compared to the porosity range assigned to the

alteration rim of the different transport classes in TURVA-2012, which is 2–5% (Posiva 2013, Tables 7-13 to 7-15).

### Alteration rim effective diffusivity

Within the Forsmark site investigation a few drill core samples, taken from locations within a metre of logged hydraulically conductive features, have been subjected to laboratory through-diffusion experiments (Selnert et al. 2008). Tritiated water has been used as the tracer. These samples have been identified in this present report by comparing the tabulated borehole positions of the samples in Selnert et al. (2008, Appendix 2) with the positions of flow anomalies detected by the Posiva flow log.

This can be exemplified by borehole KFM02A. According to Selnert et al. (2008, Appendix 2), 25 drill core samples from this borehole have been subjected to through-diffusion experiments. If crosschecking the positions of these samples by the positions of detected flow anomalies interpreted as fractures in Rouhiainen and Pöllänen (2004, Appendix 7.1), one can see that only two of the samples are taken from within a metre of a hydraulically conductive fracture. These two positions have been crosschecked with the Wellcad diagram associated with the boremap mapping of the drill core of borehole KFM02A (Petersson et al. 2003, Appendix 2). From this diagram one can see that at one of these positions, the rock matrix is altered and the alteration is classified as "medium intensity, oxidised". At the other position, the rock matrix is unaltered. This routine has been repeated for all boreholes from which samples have been taken and subjected to through-diffusion experiments. In total, seven of these samples have been identified. The effective diffusivity, as well as the capacity factor (that should equal the porosity for the non-sorbing tracer HTO), of these samples are compiled in Table 4.

**Table 4. Effective diffusivity and capacity factor of Forsmark samples taken in the vicinity of flowing fractures. Diffusion data reproduced from Selnert et al. (2008, Appendix 2).**

| Borehole | Borehole length of sample | Borehole length of flowing fractures | Rock type | Alteration type of borehole section | Effective diffusivity $D_e$ ($m^2/s$) | Capacity factor $\alpha$ (-) |
|---|---|---|---|---|---|---|
| KFM02A | 300.96-300.99 | 299.4-301.7 | 101057 | Medium intensity, oxidised | $7.5 \cdot 10^{-13}$ | $2.8 \cdot 10^{-2}$ |
| KFM02A | 481.01-481.04 | 480.4-481.2 | 101057 | Unaltered | $5.80 \cdot 10^{-14}$ | $2.5 \cdot 10^{-3}$ |
| KFM04A | 359.45-359.48 | 358.2-359.8 | 101051 | Weak to medium intensity, oxidized or chloritisized | $7.9 \cdot 10^{-12}$ | $7.2 \cdot 10^{-2}$ |
| KFM05A | 168.34-168.37 | 167.2-168.7 | 101057 | Unaltered | $9.8 \cdot 10^{-14}$ | $1.6 \cdot 10^{-3}$ |
| KFM06A | 331.72-331.75 | 330.0-332.0 | 101057 | Intensity unknown, oxidized | $1.62 \cdot 10^{-12}$ | $5.13 \cdot 10^{-3}$ |
| KFM06A | 331.78-381.81 | 330.0-332.0 | 101057 | Intensity unknown, oxidized | $1.2 \cdot 10^{-12}$ | $1.85 \cdot 10^{-2}$ |
| KFM08A | 412.30-412.33 | 411.6-413.1 | 101057 | Medium or strong intensity, oxidation or quartz dissolution | $1.4 \cdot 10^{-13}$ | – |

Rock type 101057 = Granite to granodiorite, metamorphic, medium-grained
Rock type 101051 = Granite, granodiorite and tonalite, metamorphic, fine- to medium-grained

In Vilks et al. (2005), another campaign of performing laboratory diffusion experiments on samples taken from the vicinity of a hydraulically conductive fracture is reported.

The samples were taken from the drill core of the LTDE-SD[9] borehole at Äspö, where the borehole intersects the investigated fracture. The positions of the samples in the drill core, relative to the fracture surface, are provided in Figure 20. This figure also provides the resulting porosity and effective diffusivity profiles, relative to the distance from the fracture surface. Both iodide and titrated water were used as tracers.

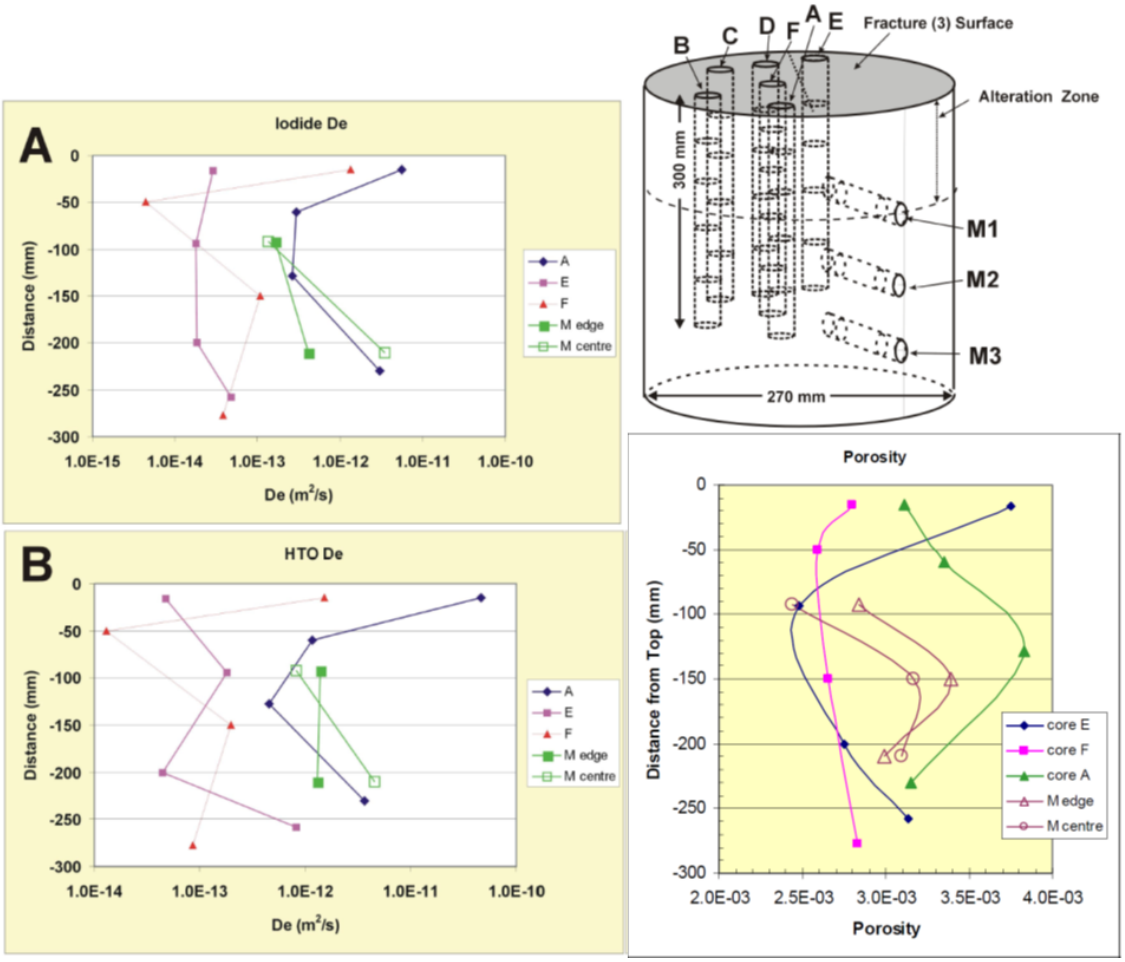


*Figure 20. Positions of samples in the drill core, as well as resulting porosity and effective diffusivity profiles relative to the LTDE-SD fracture surface. Reproduced from Vilks et al. (2005, Figures 5, 12, and 13).*

As can be seen from the above effective diffusivity data, they range over almost four orders of magnitude. Furthermore, they represent a samples volume that, to the great majority, is located further away from the fracture surface than the above specified 0.5 to 2 cm. To add to the problematic task of assigning effective diffusivities to the alteration rim, there is no information on what reduction factor should be used to account for the stress release and mechanically induced damage that the laboratory samples have suffer prior to measurements.

To deal with these problems, a subjectively chosen set of operations have been performed. First, the effective diffusivity data of Table 4 and the numerical data behind the experimental data points in the plot labelled "B" in Figure 20 (cf. Vilks et al. 2005, Table 2) have been pooled. The arithmetic mean of these effective diffusivity data is $3 \cdot 10^{-12}$ m$^2$/s. The reason for the averaging is that in radionuclide retention modelling, flowpath averaged values are used. Here it should be noted that these data represent the

[9] Long term diffusion experiment

tracer HTO at laboratory temperature, with a $D_w$ of about $2 \cdot 10^{-9}$ m$^2$/s. In SR-Site, a typical $D_w$ value of $1 \cdot 10^{-9}$ m$^2$/s has been used for the geosphere at the in-situ temperature, for all species. After scaling, this would reduce the arithmetic mean of the discussed effective diffusivities to $1.5 \cdot 10^{-12}$ m$^2$/s. A reduction factor of 4 has subjectively been chosen for stress release and mechanically induced damage. The reason why the reduction factor of 11.5 is not used, as used in SR-Site for the undisturbed rock matrix (SKB 2010c, Figure 6-80), is that some of the stress release has probably already occurred in situ, in the close vicinity of the fracture. If implementing this reduction factor, $D_e$ becomes $4 \cdot 10^{-13}$ m$^2$/s. This value is used for the moderate alteration rim of fracture class 1:1 and 1:3. This value is about 20 times higher than for the undisturbed rock. For the weakly altered rock of fracture class 1:2, it is subjectively chosen that the $D_e$ of the undisturbed rock is multiplied by a factor of five, resulting in an effective diffusivity of $1 \cdot 10^{-13}$ m$^2$/s. For the strongly altered rock of fracture class 2:1, it is assumed that the effective diffusivity is twice the assumed value of the moderate alteration rim. Consequently, the effective diffusivity for fracture class 2:1 becomes $8 \cdot 10^{-13}$ m$^2$/s.

It is fully acknowledged that other strategies could have been employed to assign effective diffusivities to the alteration rim. It is also acknowledged that in the absence of a dedicated experimental program that properly investigates the issue; only educated guesses can be provided on subject. In TURVA-2012, effective diffusivities for the alteration rim, for the different transport classes, range between $3 \cdot 10^{-13}$ and $1 \cdot 10^{-12}$ m$^2$/s (Posiva 2013, Tables 7-13 to 7-15). This is in line with our estimated range.

### Parameters of the undisturbed rock layers

Out of the 11 layers in Figure 5, four are identical layers for the undisturbed rock matrix. The undisturbed rock matrix is very well examined for site specific rock in the work leading up to SR-Site, and accordingly the SR-Site parameterisation has been used. The data have been compiled in Table 5.

**Table 5. Parameter values for undisturbed rock, all fracture classes.**

| Parameter | Value | Source/comment |
|---|---|---|
| Layer thickness | Infinite | In SR-Site, the pore connectivity was assumed to be infinite and the maximum penetration depth was set to 12.5 m (SKB 2010c, Section 6.7.10) to reflect half the spacing between hydraulically conducting fractures. For the purpose of this modelling, and for the modelled flowpaths, radionuclides will only penetrate a short distance into the rock matrix, compared to 12.5 m. Accordingly, the matrix can be considered to be infinite. |
| Rock porosity | 0.18% | Taken from SKB (2010c, Table 6-90). |
| Effective diffusivity | $2.1 \cdot 10^{-14}$ m$^2$/s | Taken from best estimate value of SKB (2010c, Table 6-91). |
| Anion exclusion factor | $\sqrt{10}$ | Taken from SKB (2010c, Table 6-91 and Section 6.8.11). Only to be applied to the effective diffusivity and not to the porosity. |

### Anion exclusion factor of fracture coatings and alteration rim

As shown in Table 5, the anion exclusion factor of $\sqrt{10}$ was assigned to the effective diffusivity in undisturbed rock. This reduction factor has been adopted for all layers of Figure 5, except for the calcite fracture coating layer of fracture class 1:3. Calcite,

which is a carbonate, has different charge properties compared to silicates and oxides. In case of calcite, the counter ions are hypothesised to be tightly bound to the surface in a very thin and non-diffuse double layer (e.g. Fenter et al. 2000). Based on this, the process of anion exclusion is assumed not to take place in this layer. Accordingly, the anion exclusion factor is set to 1.